# UC San Diego

## UC San Diego Previously Published Works


### Title

In Vivo Target Gene Activation via CRISPR/Cas9-Mediated Trans-epigenetic Modulation.


### Permalink

https://escholarship.org/uc/item/21w6j8kd



### Journal

Cell, 171(7)



### Authors

Liao, Hsin-Kai
Hatanaka, Fumiyuki
Araoka, Toshikazu
et al.



### Publication Date

2017-12-14

### DOI

10.1016/j.cell.2017.10.025

Peer reviewed



eScholarship.org Powered by the California Digital Library
University of California

Author Manuscript

Author Manuscript

Author Manuscript

Author Manuscript

HHS Public Access

Author manuscript

*Cell*. Author manuscript; available in PMC 2018 December 14.

Published in final edited form as:

*Cell*. 2017 December 14; 171(7): 1495–1507.e15. doi:10.1016/j.cell.2017.10.025.

# *In Vivo* Target Gene Activation via CRISPR/Cas9-Mediated *Trans*-Epigenetic Modulation

**Hsin-Kai Liao**[1,*], **Fumiyuki Hatanaka**[1,*], **Toshikazu Araoka**[1,2,*], **Pradeep Reddy**[1], **Min-Zu Wu**[1], **Yinghui Sui**[3], **Takayoshi Yamauchi**[1], **Masahiro Sakurai**[1], **David O'Keefe**[1], **Estrella Nuñez**[2], **Pedro Guillen**[4], **Josep M. Campistol**[5], **Cheng-Jang Wu**[6], **Li-Fan Lu**[6], **Concepcion Rodriguez Esteban**[1], and **Juan Carlos Izpisua Belmonte**[1,#]

[1]Gene Expression Laboratory, Salk Institute for Biological Studies, La Jolla, California 92037, USA

[2]Universidad Catolica, San Antonio de Murcia, Campus de los Jeronimos, 135, Guadalupe 30107, Spain

[3]Department of Pediatrics and Cellular and Molecular Medicine, University of California, San Diego, La Jolla, CA 92093, USA

[4]Fundacion Pedro Guillen, Clinica CEMTRO, Avenida Ventisquero de la Condesa, 42, 28035 Madrid, Spain

[5]Hospital Clinic of Barcelona, Carrer Villarroel, 170, 08036 Barcelona, Spain

[6]Division of Biological Sciences, University of California, San Diego, La Jolla, California 92037, USA

## SUMMARY

Current genome-editing systems generally rely on the creation of DNA double-strand breaks (DSBs). This may limit their utility in clinical therapies, as unwanted mutations caused by DSBs can have deleterious effects. The CRISPR/Cas9 system has recently been repurposed to enable target gene activation, allowing regulation of endogenous gene expression without creating DSBs. However, *in vivo* implementation of this gain-of-function system has proven difficult. Here we report a robust system for *in vivo* activation of endogenous target genes through *trans*-epigenetic remodeling. The system relies on recruitment of Cas9 and transcriptional activation complexes to target loci by modified single guide RNAs. As proof-of-concept, we used this technology to treat several mouse models of human diseases. Results demonstrate that CRISPR/Cas9-mediated target gene activation can be achieved *in vivo*, leading to observable phenotypic changes, and

[#]Correspondence: Juan Carlos Izpisua Belmonte, belmonte@salk.edu.
[*]These authors contributed equally to this work

**Publisher's Disclaimer:** This is a PDF file of an unedited manuscript that has been accepted for publication. As a service to our customers we are providing this early version of the manuscript. The manuscript will undergo copyediting, typesetting, and review of the resulting proof before it is published in its final citable form. Please note that during the production process errors may be discovered which could affect the content, and all legal disclaimers that apply to the journal pertain.

**AUTHOR CONTRIBUTIONS**

H.-K.L., F.H., T.A., and J.C.I.B. designed all experiments. H.-K.L., F.H., T.A., P.R., D.O., and J.C.I.B. prepared the figures and wrote the manuscript. H.-K.L., F.H., T.A., P.R., M.-Z.W, Y.S., T.Y., M.S., E.N., C.R.E. performed and/or analyzed *in vitro* experiments. H.-K.L., F.H., T.A., P.R., C.-J.W., L.-F.L., P.G., J.M.C. performed and/or analyzed *ex vivo* and/or *in vivo* experiments.

Author Manuscript Author Manuscript Author Manuscript Author Manuscript

amelioration of disease symptoms. This establishes new avenues for developing targeted epigenetic therapies against human diseases.

## Graphical Abstract

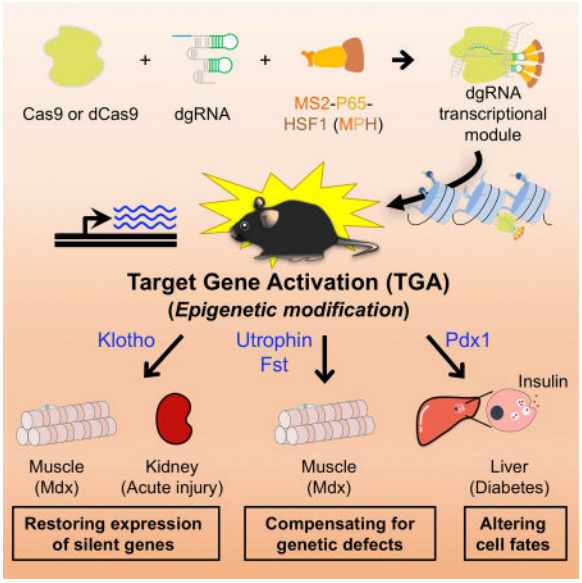


## INTRODUCTION

Over the past 30 years, epigenetic therapies have been developed to treat many human diseases, including cancer, diabetes, autoimmunity, and genetic disorders (Heerboth et al., 2014; Pfister and Ashworth, 2017). Most of these approaches have relied on drugs that ubiquitously alter epigenetic marks (e.g., DNA methylation or histone modifications). However, these epi-drugs are not without risk, as off-target genes may be affected (Altucci and Rots, 2016; Hunter, 2015). Therefore, it is important to establish new methods for generating targeted epigenetic modifications to alter the expression of specific genes (de Groote et al., 2012; Jurkowski et al., 2015; Takahashi et al., 2017).

Advances in genome editing technologies have revolutionized a wide range of scientific fields, from basic sciences to translational medicine. In particular, discovery of the bacterial immune system, CRISPR/Cas9, has led to the development of tools for rapid and efficient RNA-based, sequence-specific genome editing (Jinek et al., 2012). In addition to enabling the engineering of eukaryotic genomes, recent alterations to the CRISPR/Cas9 system have provided opportunities for regulating gene expression and for creating epigenetic alterations, without introducing DNA double-strand breaks (DSBs) (Qi et al., 2013). This avoids the concern of creating undesired permanent mutations in target genomes. Original efforts to convert the CRISPR/Cas9 gene editing system into a transactivator were achieved by fusing a transcriptional activation domain (VP64) to versions of Cas9 that lacked nuclease activity (dCas9) (Gilbert et al., 2013; Perez-Pinera et al., 2013). This enabled the CRISPR/Cas9 system to transcriptionally activate target genes within the native chromosomal context. This transformative technology has the potential to provide the foundation for many scientific and

Author Manuscript Author Manuscript Author Manuscript Author Manuscript

medical applications, including: 1) performing functional genetic screens, 2) creating synthetic gene circuits, 3) developing therapeutic interventions to compensate for genetic defects, and 4) redirecting cell fate by epigenetic reprogramming for regenerative medicine (Chen and Qi, 2017; Thakore et al., 2016; Vora et al., 2016).

The original version of the dCas9-VP64 system was unable to stimulate robust target gene activation (TGA) by using a single guide RNA (sgRNA). In most cases, TGA efficiency relied on the recruitment of multiple sgRNAs to the target gene (Gilbert et al., 2013; Kearns et al., 2014), diminishing the utility of this epigenetic tool. To improve the efficiency of CRISPR/Cas9-mediated TGA, multiple transcriptional activation domains were fused or recruited to the dCas9/gRNA complex (e.g., tripartite activator system (dCas9-VPR), synergistic activation mediator (SAM), or dCas9-Suntag) (Chavez et al., 2015; Konermann et al., 2015; Tanenbaum et al., 2014). These second-generation CRISPR/Cas9 TGA systems proved effective for functional genetic studies by single gRNAs *in vitro*, but using them *in vivo* remains a challenge (Komor et al., 2017; Thakore et al., 2016). This is primarily because of insufficient transduction of the Cas9 fusion protein *in vivo*, and low levels of *in vivo* TGA. In addition, sequences encoding the dCas9/gRNA and co-transcriptional activator complexes exceed the capacity of most common viral vectors (e.g., adeno-associated virus (AAV)), which represent the most promising method for gene delivery *in vivo* (Komor et al., 2017; Thakore et al., 2016).

To our knowledge, current CRISPR/Cas9-mediated epigenetic editing systems have not yet been able to induce a physiologically relevant phenotype in a postnatal mammal (Jurkowski et al., 2015; Vora et al., 2016). This limits the utility of these tools for performing experiments and for developing targeted epigenetic therapies. In this study, we first identified a combination of co-transcriptional activators and sgRNAs that fit within a single AAV vector and induced high levels of TGA. Injection of these single AAVs (AAV-gRNA) into Cas9-expressing mice (Platt et al., 2014) resulted in efficient TGA and clear phenotypes, thus expanding the utility of Cas9-mice to conducting gain-of-function studies *in vivo*. Next, we used this optimized system to ameliorate disease phenotypes (namely, acute kidney injury, type 1 diabetes, and the *mdx* model of Duchenne muscular dystrophy) by introducing Cas9 transgenes into these disease mouse models. Finally, we generated a dual-AAV system and showed that co-injection of AAV-Cas9 with an AAV-gRNA that targeted *utrophin* could ameliorate the muscular dystrophy symptoms of *mdx* mice. In summary, we have developed an *in vivo* CRISPR/Cas9 TGA system for activating the expression of endogenous genes. This system can induce epigenetic remodeling of targeted loci by recruiting the transcriptional machinery (a process we call *trans*-epigenetic modulation), and can potentially be used to treat a wide range of human diseases and injuries.

## RESULTS

### An Optimized CRISPR/Cas9 System Enables Target Gene Activation

To date, all second-generation CRISPR/Cas9 TGA systems have fused nuclease dead Cas9 (dCas9) to a transcriptional activation complex. This inevitably results in a coding sequence that exceeds the capacity of a single AAV. We therefore sought to develop a system in which

Author Manuscript Author Manuscript Author Manuscript Author Manuscript

the transcriptional activators were separated from dCas9. To this end, we adapted the SAM module from second-generation CRISPR/Cas9-based TGA systems (Konermann et al., 2015). The SAM system relies on an engineered hairpin aptamer that contains two MS2 domains, which can recruit the MS2:P65:HSF1 (MPH) transcriptional activation complex to the target locus. This separate, MS2-mediated, transactivation complex significantly enhances the efficiency of TGA for dCas9-VP64. However, the dCas9-VP64 construct still exceeds the capacity of regular AAVs. To solve this issue, we instead used short sgRNAs (14 or 15 base pairs (bp) rather than 20 bp) to guide wild-type Cas9 to the target locus. Importantly, these short sgRNAs prevent active Cas9 from creating a DSB (Dahlman et al., 2015; Kiani et al., 2015), and are therefore termed dead sgRNAs (dgRNAs). We used versions of dgRNAs engineered to contain two MS2 domains for recruiting the MPH transcriptional activation complex (Dahlman et al., 2015). Here we refined the dgRNA system to enable high levels of *in vivo* TGA when introduced into mice expressing active Cas9 (Figure 1A) (Platt et al., 2014).

As a first step toward improving the CRISPR/Cas9-dgRNA system, we constructed a luciferase reporter that included a dgRNA binding site followed by a minimal promoter and a luciferase expression cassette (the tLuc reporter) (Figure 1B). We then systematically altered MS2 dead sgRNA (MS2dgRNAs) sequences targeting tLuc and screed for high levels of luciferase activity *in vitro*. (Figures 1C and S1A). Our strategy was to optimize the MS2dgRNA scaffold by changing the GC ratio, or by shortening repetitive sequences, or both. Based on these *in vitro* analyses, 14bp-TCAG-MS2dgLuc provided highest level of reporter activation (Figures 1D and S1B). Strikingly, activation efficiency of the optimized dgRNA system was comparable to that seen with the original dCas9VP64 in combination with MPH (dCas9VP64/MPH/MS2gLuc). Thus, even without VP64, the modified Cas9/MS2dgLuc-MPH complex drove high levels of TGA (Figure 1E). This was encouraging, as it suggested that we might be able to induce high levels of TGA using an AAV-Cas9 (without VP64) *in vivo*. We tested other combinations of transcriptional activation complexes (e.g., VP64, P65, and Rta), but the MPH complex was most effective (Figures S1C–S1F) (Chavez et al., 2015; Chavez et al., 2016; Konermann et al., 2015).

To test the efficacy of our optimized system in live animals, plasmids containing the luciferase reporter and plasmids containing dgLuc/MPH sequences (dgLuc will be used to represent optimized MS2dgLuc) were co-injected into hind-limb muscles of adult Cas9-expressing mice. Plasmids were electroporated into muscle cells and luciferase activity monitored 9 days later (Figure 1F). The dgLuc/MPH system resulted in luciferase expression, whereas replacing dgLuc with gLuc (i.e., one with a full-length target sequence) resulted in no luciferase activity (Figure 1G).

## An AAV-Mediated CRISPR/Cas9 TGA System Activates Reporters in Different Organs of Mice

To facilitate the *in vivo* delivery of our CRISPR/Cas9 TGA system, and to potentially elevate expression levels, we introduced elements of the system (namely dgLuc and MPH) into an AAV, in which dgLuc and MPH expressions were driven by the U6 and CAG promoters, respectively (AAV-dgLuc-CAG-MPH). We chose AAV serotype 9 because it

Author Manuscript Author Manuscript Author Manuscript Author Manuscript

infects a wide range of organs, and is therapeutically safe (Zincarelli et al., 2008). To assess levels of TGA, we created a reporter AAV in which luciferase and mCherry sequences were placed downstream of the dgLuc binding site (AAV-tLuc-mCherry; Figure 2A). We then bilaterally co-injected these two AAVs into hind-limb muscles of Cas9-expressing neonatal mice (P2.5) and assessed luciferase activity at P15 (Figure 2B). Co-injection of these AAVs resulted in luciferase activity *in vivo*, but not when a scrambled dgRNA control (dgMock) was used (Figure 2C). We next injected the AAVs directly into the brain of Cas9-expressing mice and again detected CRISPR/Cas9-mediated TGA (injections were performed at P0.5 and luciferase activity assessed at P21) (Figures 2D and 2E). Next, the AAVs were delivered systemically via facial vein injection into Cas9-expressing mice at P0.5. At P21, mice injected with AAV-dgLuc exhibited luciferase activity, but not those injected with AAV-dgMock (or non-injection controls) (Figures 2F and 2G). Organs were dissected from mice injected with AAV-dgLuc and highest levels of *ex vivo* luciferase activity were detected in the liver and heart. Lower levels were detected in the lung, kidney, muscle, spinal cord, and stomach (Figure 2H). Finally, the AAVs were systemically delivered to adult mice via tail vein injection (Figure 2I). Four days later, luciferase activity was detected in the liver of mice receiving AAV-dgLuc, but not AAV-dgMock (or non-injection controls) (Figure 2J). These results demonstrate our optimized CRISPR/Cas9 TGA system can induce transcription of a reporter gene *in vivo*.

## Phenotypic Enhancement of Muscle Mass Induced by *In Vivo* CRISPR/Cas9 TGA

The next critical test of the CRISPR/Cas9 TGA system was to activate an endogenous gene (rather than an exogenous reporter), and to determine whether induced levels of expression were sufficient to cause a phenotype. We targeted the mouse *follistatin* (*Fst*) gene because *Fst* overexpression increases muscle mass (Haidet et al., 2008). We and others have found that TGA is most effective when sgRNAs target sequences within −400 and +100 bp of the transcriptional start site (in particular between −100 and +50 bp) (Gilbert et al., 2014; Kearns et al., 2014; Konermann et al., 2015). We therefore constructed dgFst RNAs based on these data and identified two *Fst* target sequences (T1 and T2) near the transcriptional start site. To test *Fst* activation *in vitro*, N2a cells stably expressing Cas9 were transfected with dgFst-T1-MPH or dgFst-T2-MPH plasmids. Controls included dgMock-MPH and a no transfection group. Comparable levels of *Fst* expression (~50-fold up-regulation compared to controls) were seen with the two dgFst-MPH constructs (Figure 3A). AAV-dgFst-T2-MPH was then delivered via intramuscular (IM) injection into the hind-limb of Cas9-expressing mice at P2.5 (Figure 3B). At P21, increased levels of *Fst* expression (~18-fold compared to gMock controls) were seen in hind-limbs injected with AAV-dgFst-T2-MPH (Figure 3C). At P45, a gross increase in muscle mass was observed (Figure 3D). Increases in *Fst* expression and muscle mass were still observed 3 months following the injections (Figures 3C, 3E and 3F). AAV-dgFst-T2-MPH injection increased muscle fiber size in the tibialis anterior (TA) muscle (Figures 3G–3I), and increased hind-limb muscle strength compared with controls. Less or no difference in the strength of fore limbs, which were not injected, was observed in these animals (Figure 3J).

To determine the effect on *Fst* expression when the AAV was delivered systemically, AAV-dgFst-T2-MPH was administered to Cas9-expressing mice at P0.5 via facial vein injection.

Author Manuscript Author Manuscript Author Manuscript Author Manuscript

At P21, heart, liver, and muscle tissues were dissected and *Fst* expression was analyzed (Figure S2A). *Fst* expression levels were elevated 45-fold, 9-fold, and 2.7-fold in heart, liver, and muscle tissues, respectively (compared with control PBS-injected mice) (Figure S2B). Twelve weeks after the injection, increases in muscle fiber size were observed in the TA and quadriceps femoris (QF) muscles, compared to PBS controls (Figures S2C–S2E). Finally, 12 weeks after the injection, *Fst* overexpression led to increases in the relative weights of the TA and QF muscles (Figure S2F).

## Induction of IL-10 or Klotho Expression via *In Vivo* CRISPR/Cas9 TGA can Ameliorate Acute Kidney Injury

To demonstrate potential therapeutic applications of CRISPR/Cas9 TGA, we next asked whether our system could ameliorate mouse models of human diseases. We first used a mouse model of acute kidney injury, targeting the genes *klotho* and *interleukin 10* (*Il10*). Klotho protects against renal damage, and expression of this gene is reduced following ageing and acute kidney injury (Figure S3A) (Kurosu et al., 2005; Panesso et al., 2014). IL-10 is an anti-inflammatory cytokine that ameliorates renal injury following cisplatin treatment (Jin et al., 2013; Ling et al., 2011). We asked whether the CRISPR/Cas9 TGA system could be used to induce the expression of Klotho or IL-10 *in vivo* to treat acute kidney injury. For these experiments, we first derived mouse embryonic stem cell lines from Cas9-expressing mice (Cas9 mESCs) and used them to examine gene induction by dgRNAs targeting *klotho* or *Il10* (Figures S3B and S3C). The most effective *klotho* and *Il10* dgRNAs from these *in vitro* assays were then assembled into AAV vectors (AAV-dgKlotho-MPH and AAV-dgIL-10-MPH), and viruses were injected into the tail vein of adult Cas9 mice (Figure 4A). We first assessed the specificity of *in vivo* TGA using RNA-seq. Twelve days following the injection, liver tissue was dissected. Compared to AAV-dgMock controls, target genes were dramatically upregulated (158-fold for *Il10*, and 2553-fold for *klotho* on average), indicating high levels of TGA *in vivo* (Figure S3D). In addition, mice injected with AAV-dgIL-10-MPH exhibited no induction of *klotho* (and vice versa), indicating no crosstalk between these reagents. Next, to address the concern that truncated dgRNAs were causing DSBs in the presence of active Cas9, we transduced either sgRNAs or MS2-dgRNAs together, and analyzed by Surveyor assay and deep sequencing. Results showed that sgRNAs disrupted target genes (via DSB-induced indel generation), whereas MS2-dgRNAs induced TGA with undetectable levels of DSBs (*in vitro* and *in vivo* samples) (Figures S3E–S3K).

To assess therapeutic benefit, acute kidney injury was induced in mice via cisplatin injection 8 days after AAV injection (Figure 4A). AAV injection elevated levels of *klotho* and *Il10* gene expression in the liver (Figure 4B), and elevated levels of Klotho protein that was secreted into the serum (Figure 4C). Overexpression of Klotho or IL-10 in cisplatin-treated mice resulted in improved renal function, as blood urea nitrogen (BUN) and serum creatinine (S-Cre) levels were significantly lower compared to dgMock controls (Figure 4D). Moreover, kidneys from these mice were dissected and histologically analyzed. Overexpressing Klotho or IL-10 improved a number of pathological features (namely tubular necrosis, tubular dilation, urinary cast, and loss of tubular borders) compared with controls (Figures 4E and 4F). Importantly, AAV treatment extended mouse survival time following a high dose of cisplatin treatment; this effect was most dramatic with Klotho

Author Manuscript Author Manuscript Author Manuscript Author Manuscript

(Figure 4G). Thus, the CRISPR/Cas9 TGA system induced the expression of functional proteins *in vivo*, and levels of Klotho/IL-10 overexpression were sufficient to provide prophylactic interventions of disease pathogenesis in a mouse model of acute kidney injury.

## CRISPR/Cas9 TGA Results in *In Vivo* Transdifferentiation of Liver Cells into Insulin-Producing Cells via *Trans*-Epigenetic Modulation

Next, we asked whether activation of an endogenous gene via CRISPR/Cas9-mediated TGA could lead to *in vivo* transdifferentiation of cells. To test this idea, we sought to overexpress *pancreatic and duodenal homeobox gene 1* (*Pdx1*) in liver cells (using AAV-dgPdx1-MPH) with the goal of generating insulin-secreting cells to treat a mouse model of type I diabetes. Pdx1 is necessary for pancreatic development and can transdifferentiate hepatocytes into pancreatic beta-like insulin-producing cells (Ferber et al., 2000; Tang et al., 2006). We first identified effective dgRNAs against *Pdx1* using Cas9 mESCs *in vitro*. Injecting AAV-dgPdx1-MPH into adult Cas9-expressing mice via tail vein injection elevated levels of *Pdx1* in liver cells, compared to dgMock controls (Figures 5A–5C and 5F). In addition to overexpressing *Pdx1*, AAV-dgPdx1-MPH resulted in the upregulation of *insulin 1* (*Ins1*), *insulin 2* (*Ins2*), and *proprotein convertase subtilisin/kexin type 1* (*Pcsk1*) in liver cells; the latter participates in insulin processing (Figures 5D, 5E and S4A).

To test if our *in vivo* TGA system also affected epigenetic marks near the targeted genomic locus, chromatin-immunoprecipitation (ChIP)-qRT-PCR of liver samples from mice injected with AAV-dgPdx1-MPH was performed. H3K4me3 and H3K27ac epigenetic marks, which are typically associated with transcriptionally active genes, were enriched at the *Pdx1* locus of AAV-dgPdx1-MPH injected mice, compared to AAV-dgMock controls (Figures 5G–5I). These patterns of epigenetic modifications were similar to those seen in Pdx1-expressing tissues (e.g., small intestine) (Figure 5G). Thus, the CRISPR/Cas9 TGA system transcriptionally activated a gene that is normally silent in a target organ via the *trans*-epigenetic remodeling of histone marks.

Importantly, when mice were administered AAV-dgPdx-1-MPH two days following streptozotocin (STZ) treatment (160 mg/kg), which induces hyperglycemia and creates a mouse model of type I diabetes, treated mice exhibited lower blood glucose levels than dgMock controls, partially rescued STZ-induced hyperglycemia (Figure S4B). In addition, serum insulin levels were higher in STZ-treated mice that received AAV-dgPdx1-MPH (Figure S4C), indicating that the AAV treatment was indeed capable of transforming liver cells into insulin-secreting cells. The CRISPR/Cas9 TGA system may therefore provide a means of *in vivo* cell fate engineering to produce cell types necessary to restore particular physiological functions.

To further demonstrate the utility of the *in vivo* CRISPR/Cas9 TGA system, we sought to overexpress more than one gene at the same time. For this purpose, we designed dgRNAs to overexpress Six2 (AAV-dgSix2-MPH), a transcription factor expressed in the kidney (Figures S4D–S4F) (Kobayashi et al., 2008). AAV-dgPdx1-MPH and AAV-dgSix2-MPH were co-injected into the tail vein of Cas9-expressing mice. Both genes were overexpressed in the liver, indicating multiplexed *in vivo* TGA is feasible (Figure S4G). Together, these results indicated that the CRISPR/Cas9 TGA system can be used to activate multiple

Author Manuscript Author Manuscript Author Manuscript Author Manuscript

endogenous genes *in vivo* and that TGA and targeted gene knockout can be achieved simultaneously in Cas9-expressing mice.

### CRISPR/Cas9 TGA of Klotho and Utrophin Partially Rescues Dystrophin Deficient Mice

We next asked whether our system could ameliorate disease phenotype in mouse models of human genetic disorders. We choose the *mdx* mouse model of Duchenne muscular dystrophy (DMD) (Sicinski et al., 1989). DMD is a lethal, inherited muscle wasting disorder resulting from a loss-of-function mutation in the large gene, *dystrophin* (the cDNA is ~14 kb). Because of the large size of this gene, it has proven challenging to deliver a fully functional *dystrophin* transgene via traditional virus-mediated gene therapies (Janghra et al., 2016; Sicinski et al., 1989). Currently, there is no effective therapy for DMD and transplanting muscle stem cells into damaged organs to stop disease progression has proven difficult (Sienkiewicz et al., 2015). Recent studies have demonstrated that *klotho* is epigenetically silenced in muscle cells of *mdx* mice at the time of disease onset, and systemic expression of *klotho* via a transgene can relieve disease symptoms (Wehling-Henricks et al., 2016). Therefore, we injected AAV-dgKlotho-MPH into neonatal *Cas9/mdx* mutant mice via facial vein injection. This AAV restored *klotho* expression in muscle tissue (Figures S5A and S5B), increasing TA muscle mass compared to dgMock controls (Figures S5C and S5D). Two months after *Cas9/mdx* mice received AAV-dgKlotho-MPH, they showed improved muscle strength based on wire-hang and grip strength tests, compared to dgMock controls (Figures S5E and S5F). CRISPR/Cas9-mediated activation of the endogenous *klotho* gene was therefore able to ameliorate DMD phenotypes, partially rescuing this mouse model of a human genetic disorder.

An alternative way of treating DMD is to upregulate *utrophin*, as the *utrophin* and *dystrophin* genes encode very similar proteins (~80% similarity) and systemic expression of *utrophin* in a transgenic model relieves disease symptoms (Rafael et al., 1998; Tinsley et al., 1996). As with *dystrophin*, the *utrophin* cDNA is too large to package into most viral vectors for traditional gene therapy. To overcome this hurdle, we sought to use our *in vivo* CRISPR/Cas9 TGA system to activate the endogenous *utrophin* gene to compensate for the loss of *dystrophin*. We first created 18 dgRNAs to identify the most effective *utrophin* target sites (Figure 6A). Among these *utrophin* dgRNAs, T2 and T16 were most promising (Figure 6B) (Burton et al., 1999). We administered AAV-dgUtrn-T2-MPH or AAV-dgUtrn-T16-MPH via IM injection into Cas9-expressing mice; both induced *utrophin* expression in muscle compared with dgMock controls (Figures 6C–6E). We then injected AAV-dgUtrn-T2-MPH into the hind limbs of *Cas9/mdx* mice (at P2.5). Two months later, treated mice exhibited improved hind-limb grip strength compared with Cas9/*mdx* controls (untreated or AAV-dgMock-MPH). No effect on grip strength was seen for non-injected fore limbs (Figure 6F).

We next asked whether TGA-mediated up-regulation of *utrophin* could rescue *mdx* mice after the pathophysiology had been established. We injected AAV-dgUtrn-T2 and AAV-dgUtrn-T16 together into the hind limbs of 3-week-old *Cas9/mdx* and *mdx* littermates. Indeed, disease symptoms were reduced for *Cas9*/*mdx* mice, but not for *mdx* controls, which lacked Cas9 (Figure S6).

Author Manuscript Author Manuscript Author Manuscript Author Manuscript

### Amelioration of Dystrophic Phenotypes by a dual AAV-CRISPR/Cas9 TGA System that Includes AAV-Cas9

As a final step toward demonstrating the potential therapeutic utility of CRISPR/Cas9 TGA, we asked whether our optimized AAV-dgRNA-MPH could work in combination with a Cas9 AAV virus (AAV-SpCas9) to activate target genes *in vivo*. We tested a number of promoters and constructs, and determined that AAV-CMVc-SpCas9 and AAV-nEF-SpCas9 (both driven by short, ubiquitous promoters of ~500 bp) showed the best TGA efficiency. We evaluated TGA efficiency by co-injecting AAV-dgFst-T2-MPH with AAV-SpCas9 into the fore and hind limb muscles of wild-type mice at P2.5. At P21, muscles were dissected and levels of *Fst* expression were analyzed (Figure S7A). *Fst* expression was elevated 9-fold, 28-fold, and 11-fold in fore limb, TA, and QF muscles, respectively (compared with AAV-dgMock-MPH or no-injection controls) (Figure S7B). Similar levels of *Fst* overexpression were observed when AAV-SpCas9 was replaced with nuclease-dead Cas9 (AAV-SpdCas9) (Figure S7C). Using AAV-SpdCas9 would minimize the concern of generating DSBs when applying CRISPR/Cas9 TGA treatments *in vivo*. Co-injection of AAV-dgFst-MPH and AAV-SpCas9 also induced H3K4me3 and H3K27ac activation marks within *Fst* target sequences (Figures 7F and S7D–S7F). More importantly, co-injection of AAV-SpCas9 with AAV-dgFst-MPH or AAV-dgUtrn-MPH ameliorated disease symptoms of *mdx* mice compared with AAV-dgMock controls (Figure 7). These data reveal that our dual-AAV *in vivo* CRISPR/Cas9 system can efficiently induce TGA to promote therapeutic benefit.

## DISCUSSION

Regulating the epigenome represents a promising strategy for treating human diseases that have not been cured using traditional drug strategies (Heerboth et al., 2014; Hunter, 2015). Here we describe a CRISPR/Cas9 TGA system that can transcriptionally activate target genes *in vivo* by modulating histone marks rather than editing DNA sequences. Our *in vivo* CRISPR/Cas9 TGA system indirectly induced epigenetic remodeling by recruiting the transcriptional machinery, not by directly recruiting epigenetic modulators. This system altered target gene expression *in vivo* to generate physiologically relevant phenotypes without causing DSBs.

AAVs represent the most promising method for *in vivo* gene delivery. A split Cas9 AAV system, which relies on the *trans*-splicing machinery, was recently described as a way of circumventing the capacity limitation of AAV vectors (Chew et al., 2016). However, it is unclear whether modest levels of *in vivo* TGA achievable with this split system are sufficient to induce phenotypic change. The technology reported here, which utilizes a modified CRISPR/Cas9 machinery and a co-transcriptional complex, was fully able to: 1) rescue levels of gene expression (e.g., restore Klotho levels following acute kidney injury or in the *mdx* model), 2) compensate for genetic defects (e.g., overexpress Utrophin to compensate for loss of Dystrophin), and 3) alter cell fates by inducing transdifferentiation factors (e.g., generate insulin-producing cells by ectopically expressing Pdx1).

Recently, several groups have partially restored *dystrophin* gene function in models of DMD using CRISPR/Cas9 technology. Their strategy was to directly remove mutated exons to create a shortened *dystrophin* gene (Long et al., 2016; Nelson et al., 2016; Tabebordbar et

Author Manuscript Author Manuscript Author Manuscript Author Manuscript

al., 2016). This elegant approach may not be effective in other contexts, where specific exons may be essential for protein function and therefore cannot be removed to ameliorate the disease. In addition, the need to generate DSBs for this approach has the potential to create unwanted genetic mutations, a significant concern within the field of gene therapy (Schaefer et al., 2017). In contrast, our *in vivo* CRISPR/Cas9 TGA system did not generate DNA breaks. Furthermore, it has recently been shown that AAV-mediated delivery of CRISPR-Cas9 does not induce extensive cellular damage *in vivo* (Chew et al., 2016). Despite these advantages, further studies are needed before this strategy can be applied in the clinic. For example, it must be determined whether host immune responses against the AAV-CRISPR/Cas9 TGA system arise.

In summary, the *in vivo* TGA system described here can be used to transcriptionally activate endogenous genes (either single genes or combinations of genes), including extremely large genes. This system can be used to express genes to compensate for disease-associated genetic mutations, or to overexpress long non-coding RNAs oas well as GC-rich genes to reveal their biological functions, a difficult feat until now (La Russa and Qi, 2015; Vora et al., 2016). Finally, combined loss- and gain-of-function manipulations can be applied to rapidly establish epistatic relationships between genes *in vivo*. In the future, improvements in the specificity of the system by designing tissue-specific promoters, and by using AAVs with specific tropism, will enhance and widen the applicability of the system. Thus, the versatile and efficient *in vivo* CRISPR/Cas9-mediated gene activation system introduced here holds great promise, both as a tool for *in vivo* biomedical research, and as a targeted epigenetic approach for treating a wide range of human diseases.

## CONTACT FOR REAGENTS AND RESOURCE SHARING

Further information and requests for resources and reagents should be directed to and will be fulfilled by the Lead Contact Juan Carlos Izpisua Belmonte (belmonte@salk.edu).

## EXPERIMENTAL MODEL AND SUBJECT DETAILS

All animal procedures were performed according to NIH guidelines and approved by the Committee on Animal Care at the Salk Institute.

### Mice

ICR, C57BL/6, Rosa26-Cas9 knock-in (Gt(ROSA)26Sor$^{tm1.1(CAG-Cas9*,-EGFP)Fezh}$, Stock No. 024858), and Dmd$^{mdx}$ (C57BL/10ScSn-Dmd$^{mdx/}$J, Stock No. 001801) mice were purchased from the Jackson laboratory. The mice were housed in a 12-hour light/dark cycle (light between 06:00 and 18:00) in a temperature-controlled room (22 ± 1 °C) with free access to water and food. All procedures were performed in accordance with protocols approved by the IACUC and Animal Resources Department of the Salk Institute for Biological Studies. The ages of mice are indicated in each figure legend or panel. Both female and male mice were used for behavioral experiments, no notable sex-dependent differences were found in our analyses. For beta-cell ablation experiments, male mice were randomly assigned to experimental and control groups.

Author Manuscript Author Manuscript Author Manuscript Author Manuscript

### Cell Lines and Cell Culture

The HEK 293A cell line was purchased from Invitrogen (Carlsbad, CA) and maintained in DMEM medium containing 10% fetal bovine serum (FBS), 2 mM glutamine, 1% non-essential amino acids, and 1% penicillin–streptomycin. Neuro-2a (N2a) cells were originally from Sigma-Aldrich and cultured with the same medium. Cas9 mouse embryonic stem cell (Cas9 mESCs) lines were derived from blastocysts of homozygous Rosa26-Cas9 knock-in mice using previously described procedures (Czechanski et al., 2014). Cells were then maintained in $N2B27^{2ILIF}$ media on Matrigel (Cultrex) coated plates. Female Cas9 mESC cell line was used in this study. This cell line was authenticated via morphology, PCR based genotyping, and sequencing.

## METHOD DETAILS

### Plasmid Design and Construction

The luciferase reporter (tLuc) was constructed by replacing mCherry with Luciferase in the M-tdTom-SP-gT1 plasmid (Addgene 48677)(Esvelt et al., 2013) and then sub-cloning this construct into the AAV backbone construct, as AAV-tLuc. The AAV-tLuc-mCherry reporter was constructed by inserting a 2A-mCheery fragment into AAV-tLuc. The U6-dgRNA-CAG-MPH plasmid was constructed by combining U6-MS2gRNA from the plasmid sgRNA(MS2)_cloning_backbone (Addgene 61424) and the MPH transactivation domain from the plasmid lenti_MS2-P65-HSF1_Hygro (Addgene 61426) under the control of a CAG promoter. U6-dgRNA-CAG-MPH was further sub-cloned into the AAV backbone to make AAV-U6-dgRNA-CAG-MPH. Either 20 bp or 14 bp spacers of gRNAs (Table S1) were inserted into the plasmids with gRNA backbones at either the BsmBI or SapI site. The mock-gRNA target sequence was synthesized as described (Liao et al., 2015). To generate different MS2 fused transcriptional activator constructs, VP64 and Rta were amplified from the SP-dCas9-VPR plasmid (Addgene 63798), and P65 was amplified from the MS2-P65-HSF1_GFP plasmid (Addgene 61423), which were subsequently sub-cloned into a pCAG-containing plasmid under the order described in Figure S1. AAV-nEF-Cas9 was described previously (Suzuki et al., 2016). AAV-CMVc-Cas9 was constructed by replacing the Mecp2 promoter of PX551 (Swiech et al., 2015) with a core CMV promoter. AAV-nEF-dCas9 was constructed by replacing the nEF promoter of pAAV-nEF-Cas9 with dCas9 coding sequence.

### Transfection of *In Vitro* Cultured Cells

Lipofectamine 2000 or 3000 (ThermoFisher) was used to transfect HEK293 cells, N2a, and Cas9 mESCs. Transfection complexes were prepared following manufacturer's instructions.

### Luciferase-Based Reporter Assay

After harvesting luciferase-expressing cells by TrypLE Express (Life Technologies), suspended cells were transferred to 96-well plates and reagents from Dual-Glo Luciferase Assay System (Promega) were applied. The luminescent signal was quantified using a Synergy H1 Hybird Reader (BioTek) with triplicated wells per sample.

Author Manuscript Author Manuscript Author Manuscript Author Manuscript

### AAV and Lentivirus Production

AAV2/9 (AAV2 inverted terminal repeat (ITR) vectors pseudo-typed with AAV9 capsid) viral particles were generated by or following the procedures of the Gene Transfer Targeting and Therapeutics Core at the Salk Institute for Biological Studies. Lentiviral vectors were packed as described and the vesicular stomatitis virus Env glycoprotein (VSV-G) was used (Liao et al., 2015).

### *In Vivo* Muscle Electroporation

Wild type or Cas9-expressing mice were anaesthetized with intraperitoneal injection of ketamine (100 mg/kg) and xylazine (10 mg/kg). A small portion of the quadriceps muscle was surgically exposed in the hind limb. Plasmid DNA mixture (25 μg of each plasmid in 50 μl TE) was injected into the muscle using a 29-gauge insulin syringe. One minute following plasmid DNA injection, a pair of electrodes was inserted into the muscle to a depth of 5 mm to encompass the DNA injection site. Muscle was electroporated using an Electro Square Porator T820 (BTX Harvard Apparatus). Electrical stimulation was delivered in twenty pulses at 100 V for 20 ms. After electroporation, the open sites were closed by stitches and the mice were allowed to recover from the anesthesia on a 37 °C warm pad.

### Intramuscular (IM) AAV Injection

Newborn (P2.5) mice were used for intramuscular injections. The AAV mixtures (AAV9-dgRNA ($1 \times 10^{11}$ GC); AAV9-tLuc reporter ($1 \times 10^{10}$ GC)) were injected into the tibialis anterior (TA) and quadriceps femoris (QA) muscles under anesthesia. For 3-week-old mice, mice were anaesthetized with intraperitoneal injection of ketamine (100 mg/kg) and xylazine (10 mg/kg). A small portion of the quadriceps muscle was surgically exposed in the hind limb. The AAVs were injected into the TA muscle and/or the QF muscle using a 33 Gauge Hamilton syringe. After AAV injection, the skin was closed by stitches, and mice recovered on a 37 °C warm pad.

### Facial Vein AAV Injection

Newborn (P0.5) mice were used for IV injection as described (Gombash Lampe et al., 2014). The AAV mixtures (AAV9-dgRNA ($1 \times 10^{11}$ GC); AAV9-tLuc reporter ($1 \times 10^{10}$ GC)) were injected via temporal vein of the P0.5 mouse.

### Intra-Cerebral AAV Injection

Neonatal mice were used for intra-cerebral injections as described (Kim et al., 2014). The AAV mixtures (AAV9-dgRNA ($5 \times 10^{10}$ GC); AAV9-tLuc reporter ($1 \times 10^{10}$ GC)) were injected intracranially into neonatal mice.

### Tail Vein AAV Injection

C57BL/6 mice and Cas9 mice (males and females, 8 to 12 weeks old) received tail vein injection of AAV (AAV9-dgRNA ($3.5 \times 10^{12}$ GC)). Liver tissues and serum samples were collected 13 days after tail vein injections. Collected liver samples were used for qRT-PCR or fixed in 4% Paraformaldehyde (PFA), and then embedded in OCT compound after a PBS

Author Manuscript Author Manuscript Author Manuscript Author Manuscript

wash and quickly frozen in ethanol. Cryostat sections (10 μm) were labeled for Insulin, Hnf3B, Pdx1, or Six2.

### Bioluminescence Imaging (BLI)

Mice were examined at each time point after electroporation or AAV infection for BLI analysis using an IVIS Kinetic 2200 (Caliper Life sciences, now PerkinElmer). Mice were injected intraperitoneally with 150 mg/kg D-Luciferin (Syn Lab), anesthetized with isoflurane, and then images were captured within 10 minutes of D-luciferin injection.

### Cisplatin-Induced Acute Kidney Injury Mouse Model

Cas9 mice (males and females, 8 to 12 weeks old) received an intraperitoneal injection of 15 mg/kg cisplatin (Tocris Bioscience, Ellisville, Missouri) 8 days after tail vein injection of AAV. Kidney tissues and blood serum samples were collected 4 days after cisplatin administration. Blood serum was assayed for blood urea nitrogen (BUN) and serum creatinine (S-Cre) levels using commercially available assays (QuantiChrom Urea Assay Kit and QuaintChrom Creatinine Assay Kit; BioAssay Systems, Hayward, CA) as renal function parameters. Collected kidney samples were fixed in 4% paraformaldehyde (PFA) and embedded in OCT compound (Sakura Tissue-Tek) after PBS wash and quickly frozen in ethanol. Cryostat sections (10 μm) were stained with either hematoxylin and eosin (H&E) or periodic acid-Schiff's reagent (PAS). Tubular necrosis, urinary casts, tubular dilation, and tubular borders were assessed in non-overlapping fields (high power field) as described (Imberti et al., 2015; Li et al., 2016).

### Beta Cell Ablation

Induction of diabetes by high dose streptozocin (STZ) treatment was performed in Cas9 male mice that were 2–4 months old. A single STZ dose (160 mg/kg) in 0.1 M sodium citrate buffer (pH 4.5) was injected intraperitoneally after the mice were fasted for 5 hours. Forty-eight hours later, the mice were randomly grouped for injection of AAV9 with dgMock or dgPdx1 through tail vein. The blood glucose levels were measured every other day with a OneTouch Ultra 2 glucometer (OneTouch) using blood from the tail vein. The mice were sacrificed at indicated times and livers were dissected and processed for histological analysis.

### Immunohistochemistry

Tissues were harvested after transcardial perfusion using ice-cold PBS, followed by ice-cold 4% paraformaldehyde in phosphate buffer for 15 min. Tissues were dissected out and postfixed in 4% paraformaldehyde overnight at 4 °C and cryoprotected in 30% sucrose overnight at 4 °C and embedded in OCT (Sakura Tissue-Tek) and frozen on dry ice. For muscle, after tissue dissection, muscle was frozen in isopentane in liquid nitrogen. Serial sections at 10 μm were made with a cryostat and collected on Superfrost Plus slides (Fisher Scientific) and stored at −80 °C until use. Immunohistochemistry was performed as follows: sections were washed with PBS for 5 min 3 times, incubated with a blocking solution (PBS containing 2% donkey serum (or 5% BSA) and 0.3% Triton X-100) for 1 h, incubated with primary antibodies diluted in the blocking solution overnight at 4 °C, washed with PBST

Author Manuscript Author Manuscript Author Manuscript Author Manuscript

(0.2% Tween 20 in PBS) for 10 min 3 times, incubated with secondary antibodies conjugated to Alexa Fluor 488, Alexa Fluor 546, or Alexa Fluor 647 (Thermo Fisher) for 1 h at room temperature. After washing, the sections were mounted with mounting medium (DAPI Fluoromount-G, SouthernBiotech). For muscle staining, antigen retrieval process was carried out by heating the sections for 20 min at 70 °C in HistoVT One solution (Nacalai tesque) and washed two times with PBS. The primary antibodies used in this study were anti-Laminin, 1:100 (L9393, Sigma); anti-Pdx1, 1:100 (ab47267, Abcam); anti-Insulin, 1:100 (ab7842, Abcam); anti-Six2, 1:200 (11562-1-AP, Proteintech); anti-Hnf-3β, 1:100 (sc-101060, Santa Cruz) and anti-Utrophin, 1:50 (sc-15377, Santa Cruz).

### RNA Analysis

Total RNA was extracted from cells and tissue samples using either TRIzol (Invitrogen) or RNeasy Kit (Qiagen) followed by cDNA synthesis using iScript Reverse Transcription Supermix for RT-PCR (Bio-Rad). qPCR was performed using SsoAdvanced SYBR Green Supermix and analyzed using a CFX384 Real-Time system (Bio-Rad). All analyses were normalized based on amplification of human or mouse *Gapdh*. Primer sequences for qPCR are listed in Table S2.

### Enzyme-Linked Immunosorbent Assay (ELISA)

Mouse sera was subjected to ELISA assay following the standard protocol (Mouse Klotho ELISA kit, CUSABIO; Mouse IL-10 ELISA kit, Affymetrix eBioscience; Mouse Insulin ELISA kit, ALPCO). ELISA assays were performed in duplicate at three separate times, and the data are expressed as mean ± SD.

### Wire Hang Test

A single 2-mm diameter wire from a metal hanger was used in this test. The vertical distance between the wire and fall point was set at 37 cm. The mouse was lifted by the tail and allowed to grasp the middle of a metal wire with its forepaws. The hanging latency was recorded until each mouse fell. Two measurements were taken per mouse. The longest hanging time was used for statistical analysis.

### Grip Strength Test

Fore and hind limb grip strengths were assessed using a grip strength meter (Chatillon Force Measurement Systems, Largo, FL). Mice were lifted by the tail and its forepaws and backpaws were each allowed to grasp onto the steel grid attached to the apparatus. The mouse was then gently pulled across the steel grid until its grip was released. Mice were tested 5 times and the three highest measured values were averaged to calculate grip strength.

### Chromatin Immunoprecipitation (ChIP)- Quantitative PCR

ChIP procedures were modified from a previous report (Hatanaka et al., 2010). Tissues were fixed in PBS containing 0.5% formaldehyde for 15 min. Glycine was added to a final concentration of 0.125 M, and the incubation was continued for an additional 15 min. After washing the samples with ice-cold PBS, the samples were homogenized in 1 mL of ice-cold

Author Manuscript Author Manuscript Author Manuscript Author Manuscript

homogenize buffer (5 mM PIPES [pH 8.0], 85 mM KCl, 0.5% NP-40, and protease inhibitors cocktail) and centrifuged (18,000 × g, 4 °C, 5 min). The pellets were suspended in nucleus lysis buffer (50 mM Tris-HCl [pH 8.0], 10 mM EDTA, 1% SDS, protease inhibitors) and sonicated 15 times for 10 s each time at intervals of 50 s with a Sonic Dismembrator 550 (Fisher Scientific). The samples were centrifuged at 18,000 g at 4 °C for 5 min. Supernatants were diluted 10-fold in ChIP dilution buffer (50 mM Tris-HCl [pH 8.0], 167 mM NaCl, 1.1% Triton X-100, 0.11% sodium deoxycholate, protease inhibitor). Nonspecific background was removed by incubating samples with a fish sperm DNA/protein A-agarose slurry at 4 °C for 2 h with rotation. The samples were centrifuged at 1,000 g at 4 °C for 2 min, and a 0.1 volume of the recovered supernatants was stored as an input sample, whereas the rest was incubated overnight with 2 μg of indicated antibodies at 4 °C with rotation. The immunocomplexes were collected with 50 μl of a fish sperm DNA/protein A/G-agarose (sc-2003, Santa Cruz) at 4 °C for 3 h with rotation. The beads were sequentially washed with the following buffers: radioimmunoprecipitation assay (RIPA) buffer-150 mM NaCl, RIPA buffer-500 mM NaCl, and LiCl wash solution. Finally, the beads were washed twice with 10 mM Tris-HCl (pH 8.0) and 1 mM EDTA. The immunocomplexes were then eluted by the addition of 200 μl of ChIP direct elution buffer (10 mM Tris-HCl [pH 8.0], 300 mM NaCl, 5 mM EDTA, 0.5% SDS) and rotated for 15 min at room temperature and incubated for 4 h at 65 °C. The DNA was recovered by phenol-chloroform-isoamyl alcohol (25:24:1) extraction and ethanol precipitation. H3K4me3 (ab8580, Abcam), H3K27ac (MA309B, Takara), and IgG-bound DNA were used for quantitative real-time PCR (qRT-PCR). The primers were designed as Table S3.

## Surveyor Assay

The indel frequency was analyzed by surveyor assay (IDT). Briefly, samples were collected to extract genomic DNA by DNeasy Blood & Tissue kit (Qiagen). The *Il-10* or *Pdx1* locus was amplified by PCR from 100 ng of genomic DNA using LA Taq Hot Start polymerase (TaKaRa) and Il-10 primers (forward: 5’- ccagttctttagcgcttacaatgc-3’ and reverse: 5’-gcagctctaggagcatgtgg-3’) or Pdx1 primers (forward: 5’-aagctcattgggagcggttttg-3’ and reverse: 5’-gtccggaggacttccctgc-3’) in a 20 μl reaction. PCR product (200 ng) was then denatured and slowly re-annealed using a step-wise gradient temperature program in a T100 thermocyler (Bio-Rad), followed the protocol adopted from previous publications (Sanjana et al., 2012).

## DNA Library Preparation and Deep Sequencing

Il-10 primers for the Surveyor assay were used for the first round of amplifications in the nested-PCR procedure with limited PCR cycles using 100ng of genomic DNA from cultured cells or tissues. This PCR product was used for the second round of amplification in the nested-PCR procedure using primer pairs with deep sequencing adaptor (mIl10-adapter-F1: 5’-ACACTCTTTCCCTACACGACGCTCTTCCGATCTcatggtttagaagagggagga-3’ and mIl10-adapter-R1: 5’-GACTGGAGTTCAGACGTGTGCTCTTCCGATCTgagcaggcagcatagcagt-3’). The nested PCR product was purified using the QIAquick PCR Purification Kit (QIAGEN) for DNA library preparation. NEB NextUltra DNA Library Preparation kit was used to prepare the sequencing library (Illumina, San Diego, CA, USA). Adapter-ligated DNA was indexed and

Author Manuscript Author Manuscript Author Manuscript Author Manuscript

enriched by limited cycle PCR. The DNA library was validated using TapeStation (Agilent Technologies, Palo Alto, CA, USA), and was quantified using a Qubit 2.0 Fluorometer. The DNA library was quantified by real time PCR (Applied Biosystems, Carlsbad, CA, USA). The DNA library was loaded onto an Illumina MiSeq instrument (Illumina, San Diego, CA, USA). Sequencing was performed using a 2×150 paired-end (PE) configuration by GENEWIZ, Inc. (South Plainfield, NJ, USA). The MiSeq Control Software (MCS) on the MiSeq instrument conducted image analysis and base calling. The raw sequencing reads were quality and adapter trimmed using Trimmomatic-0.36. The reads were aligned to the target gene reference genome using bwa-0.7.12. The variants were called for each sample using mpileup within samtools-1.3.1 followed by VarScan-2.3.9. At least 50,000 reads per sample was analyzed and the variant frequency for the indel was set above 0.25% of total reads to compare with the region of gRNA targets.

### RNA Sequencing and Data Analysis

RNA was extracted from injected mouse liver samples and prepared for RNA sequencing with TruSeq Stranded mRNA sample Prep Kit (Illumina). Deep sequencing was performed on the Illumina HiSeq platform. Single-end 50-bp reads were mapped to the UCSC mouse transcriptome (mm9) by STAR (STAR-STAR_2.4.0f1, --outSAMstrandField intronMotif --outFilterMultimapNmax 1 --runThreadN 5), allowing up to 10 mismatches (which is the default by STAR). Only the reads aligned uniquely to one genomic location were retained for subsequent analysis. Expression levels of all genes were estimated by Cufflink (cufflinks v2.2.1,-p 6 -G $gtf_file --max-bundle-frags 1000000000) using only the reads with exact matches. Gene expression level was in rpkm. Mean gene expression level was obtained by averaging across replicates. The mean gene expression levels were then transformed by log2(rpkm+1). In R 3.3.1, Pearson's Correlation is calculated for the correlation test.

## QUANTIFICATION AND STATISTICAL ANALYSIS

### Quantification

For quantification of histological and immunohistochemistry analysis, at least three sections per tissue from 3–5 animals were analyzed using ImageJ (NIH).

### Statistical Analysis

All of the data are presented as the mean ± SD or SEM and represent a minimum of three independent experiments. Statistical parameters including statistical analysis, statistical significance, and n value are reported in the Figure legends. For *in vivo* experiments n = number of animals. For ChIP-qPCR analytic data are means ± SEM, and other data are means ± SD. For statistical comparison, we performed two-tailed Student's *t*-test. A value of $p < 0.05$ was considered significant (represented as $*p < 0.05$, $**p < 0.01$, $***p < 0.001$ or not significant (n.s.)). For serum insulin levels in blood samples, statistical analyses were carried out using Prism 6 Software (GraphPad).

## Supplementary Material

Refer to Web version on PubMed Central for supplementary material.

Author Manuscript Author Manuscript Author Manuscript Author Manuscript

## Acknowledgments

We are grateful to J. Naughton and J. Marlett for AAV production, C.-C. Liao, W.-M. Hsu, B. Li and C.-Y. Chung for programming script of CRISPR data mining, M.C. Ku, N. Hah and T. Nguyen for high-throughput sequencing, J. Wu for critical reading of the manuscript, M. Schwarz for administrative help. F.H. was partially supported by a Uehara Memorial Foundation. Work in the laboratory of J.C.I.B. was supported by The Moxie Foundation, The Leona M. and Harry B. Helmsley Charitable Trust (2012-PG-MED002), the G. Harold and Leila Y. Mathers Charitable Foundation, Fundacion Dr. Pedro Guillen, AFE, UCAM and NIH (R01 HL123755).

## References

Altucci L, Rots MG. Epigenetic drugs: from chemistry via biology to medicine and back. Clinical epigenetics. 2016; 8:56. [PubMed: 27217841]

Burton EA, Tinsley JM, Holzfeind PJ, Rodrigues NR, Davies KE. A second promoter provides an alternative target for therapeutic up-regulation of utrophin in Duchenne muscular dystrophy. Proceedings of the National Academy of Sciences of the United States of America. 1999; 96:14025–14030. [PubMed: 10570192]

Chavez A, Scheiman J, Vora S, Pruitt BW, Tuttle M, E PRI, Lin S, Kiani S, Guzman CD, Wiegand DJ, et al. Highly efficient Cas9-mediated transcriptional programming. Nature methods. 2015; 12:326–328. [PubMed: 25730490]

Chavez A, Tuttle M, Pruitt BW, Ewen-Campen B, Chari R, Ter-Ovanesyan D, Haque SJ, Cecchi RJ, Kowal EJ, Buchthal J, et al. Comparison of Cas9 activators in multiple species. Nature methods. 2016; 13:563–567. [PubMed: 27214048]

Chen M, Qi LS. Repurposing CRISPR System for Transcriptional Activation. Advances in experimental medicine and biology. 2017; 983:147–157. [PubMed: 28639197]

Chew WL, Tabebordbar M, Cheng JK, Mali P, Wu EY, Ng AH, Zhu K, Wagers AJ, Church GM. A multifunctional AAV-CRISPR-Cas9 and its host response. Nature methods. 2016; 13:868–874. [PubMed: 27595405]

Czechanski A, Byers C, Greenstein I, Schrode N, Donahue LR, Hadjantonakis AK, Reinholdt LG. Derivation and characterization of mouse embryonic stem cells from permissive and nonpermissive strains. Nature protocols. 2014; 9:559–574. [PubMed: 24504480]

Dahlman JE, Abudayyeh OO, Joung J, Gootenberg JS, Zhang F, Konermann S. Orthogonal gene knockout and activation with a catalytically active Cas9 nuclease. Nature biotechnology. 2015; 33:1159–1161.

de Groote ML, Verschure PJ, Rots MG. Epigenetic Editing: targeted rewriting of epigenetic marks to modulate expression of selected target genes. Nucleic acids research. 2012; 40:10596–10613. [PubMed: 23002135]

Esvelt KM, Mali P, Braff JL, Moosburner M, Yaung SJ, Church GM. Orthogonal Cas9 proteins for RNA-guided gene regulation and editing. Nature methods. 2013; 10:1116–1121. [PubMed: 24076762]

Ferber S, Halkin A, Cohen H, Ber I, Einav Y, Goldberg I, Barshack I, Seijffers R, Kopolovic J, Kaiser N, et al. Pancreatic and duodenal homeobox gene 1 induces expression of insulin genes in liver and ameliorates streptozotocin-induced hyperglycemia. Nature medicine. 2000; 6:568–572.

Gilbert LA, Horlbeck MA, Adamson B, Villalta JE, Chen Y, Whitehead EH, Guimaraes C, Panning B, Ploegh HL, Bassik MC, et al. Genome-Scale CRISPR-Mediated Control of Gene Repression and Activation. Cell. 2014; 159:647–661. [PubMed: 25307932]

Gilbert LA, Larson MH, Morsut L, Liu Z, Brar GA, Torres SE, Stern-Ginossar N, Brandman O, Whitehead EH, Doudna JA, et al. CRISPR-mediated modular RNA-guided regulation of transcription in eukaryotes. Cell. 2013; 154:442–451. [PubMed: 23849981]

Gombash Lampe SE, Kaspar BK, Foust KD. Intravenous injections in neonatal mice. Journal of visualized experiments : JoVE. 2014:e52037. [PubMed: 25407048]

Haidet AM, Rizo L, Handy C, Umapathi P, Eagle A, Shilling C, Boue D, Martin PT, Sahenk Z, Mendell JR, et al. Long-term enhancement of skeletal muscle mass and strength by single gene administration of myostatin inhibitors. Proceedings of the National Academy of Sciences of the United States of America. 2008; 105:4318–4322. [PubMed: 18334646]

Author Manuscript Author Manuscript Author Manuscript Author Manuscript

Hatanaka F, Matsubara C, Myung J, Yoritaka T, Kamimura N, Tsutsumi S, Kanai A, Suzuki Y, Sassone-Corsi P, Aburatani H, et al. Genome-wide profiling of the core clock protein BMAL1 targets reveals a strict relationship with metabolism. Molecular and cellular biology. 2010; 30:5636–5648. [PubMed: 20937769]

Heerboth S, Lapinska K, Snyder N, Leary M, Rollinson S, Sarkar S. Use of epigenetic drugs in disease: an overview. Genetics & epigenetics. 2014; 6:9–19. [PubMed: 25512710]

Hunter P. The second coming of epigenetic drugs: a more strategic and broader research framework could boost the development of new drugs to modify epigenetic factors and gene expression. EMBO reports. 2015; 16:276–279. [PubMed: 25662153]

Imberti B, Tomasoni S, Ciampi O, Pezzotta A, Derosas M, Xinaris C, Rizzo P, Papadimou E, Novelli R, Benigni A, et al. Renal progenitors derived from human iPSCs engraft and restore function in a mouse model of acute kidney injury. Scientific reports. 2015; 5:8826. [PubMed: 25744951]

Janghra N, Morgan JE, Sewry CA, Wilson FX, Davies KE, Muntoni F, Tinsley J. Correlation of Utrophin Levels with the Dystrophin Protein Complex and Muscle Fibre Regeneration in Duchenne and Becker Muscular Dystrophy Muscle Biopsies. PloS one. 2016; 11:e0150818. [PubMed: 26974331]

Jin Y, Liu R, Xie J, Xiong H, He JC, Chen N. Interleukin-10 deficiency aggravates kidney inflammation and fibrosis in the unilateral ureteral obstruction mouse model. Laboratory investigation; a journal of technical methods and pathology. 2013; 93:801–811. [PubMed: 23628901]

Jinek M, Chylinski K, Fonfara I, Hauer M, Doudna JA, Charpentier E. A programmable dual-RNA-guided DNA endonuclease in adaptive bacterial immunity. Science. 2012; 337:816–821. [PubMed: 22745249]

Jurkowski TP, Ravichandran M, Stepper P. Synthetic epigenetics-towards intelligent control of epigenetic states and cell identity. Clinical epigenetics. 2015; 7:18. [PubMed: 25741388]

Kearns NA, Genga RM, Enuameh MS, Garber M, Wolfe SA, Maehr R. Cas9 effector-mediated regulation of transcription and differentiation in human pluripotent stem cells. Development. 2014; 141:219–223. [PubMed: 24346702]

Kiani S, Chavez A, Tuttle M, Hall RN, Chari R, Ter-Ovanesyan D, Qian J, Pruitt BW, Beal J, Vora S, et al. Cas9 gRNA engineering for genome editing, activation and repression. Nature methods. 2015; 12:1051–1054. [PubMed: 26344044]

Kim JY, Grunke SD, Levites Y, Golde TE, Jankowsky JL. Intracerebroventricular viral injection of the neonatal mouse brain for persistent and widespread neuronal transduction. Journal of visualized experiments : JoVE. 2014:51863. [PubMed: 25286085]

Kobayashi A, Valerius MT, Mugford JW, Carroll TJ, Self M, Oliver G, McMahon AP. Six2 defines and regulates a multipotent self-renewing nephron progenitor population throughout mammalian kidney development. Cell stem cell. 2008; 3:169–181. [PubMed: 18682239]

Komor AC, Badran AH, Liu DR. CRISPR-Based Technologies for the Manipulation of Eukaryotic Genomes. Cell. 2017; 168:20–36. [PubMed: 27866654]

Konermann S, Brigham MD, Trevino AE, Joung J, Abudayyeh OO, Barcena C, Hsu PD, Habib N, Gootenberg JS, Nishimasu H, et al. Genome-scale transcriptional activation by an engineered CRISPR-Cas9 complex. Nature. 2015; 517:583–588. [PubMed: 25494202]

Kurosu H, Yamamoto M, Clark JD, Pastor JV, Nandi A, Gurnani P, McGuinness OP, Chikuda H, Yamaguchi M, Kawaguchi H, et al. Suppression of aging in mice by the hormone Klotho. Science. 2005; 309:1829–1833. [PubMed: 16123266]

La Russa MF, Qi LS. The New State of the Art: Cas9 for Gene Activation and Repression. Molecular and cellular biology. 2015; 35:3800–3809. [PubMed: 26370509]

Li Z, Araoka T, Wu J, Liao HK, Li M, Lazo M, Zhou B, Sui Y, Wu MZ, Tamura I, et al. 3D Culture Supports Long-Term Expansion of Mouse and Human Nephrogenic Progenitors. Cell stem cell. 2016; 19:516–529. [PubMed: 27570066]

Liao HK, Gu Y, Diaz A, Marlett J, Takahashi Y, Li M, Suzuki K, Xu R, Hishida T, Chang CJ, et al. Use of the CRISPR/Cas9 system as an intracellular defense against HIV-1 infection in human cells. Nature communications. 2015; 6:6413.

Author Manuscript Author Manuscript Author Manuscript Author Manuscript

Ling GS, Cook HT, Botto M, Lau YL, Huang FP. An essential protective role of IL-10 in the immunological mechanism underlying resistance vs. susceptibility to lupus induction by dendritic cells and dying cells. Rheumatology. 2011; 50:1773–1784. [PubMed: 21727182]

Long C, Amoasii L, Mireault AA, McAnally JR, Li H, Sanchez-Ortiz E, Bhattacharyya S, Shelton JM, Bassel-Duby R, Olson EN. Postnatal genome editing partially restores dystrophin expression in a mouse model of muscular dystrophy. Science. 2016; 351:400–403. [PubMed: 26721683]

Nelson CE, Hakim CH, Ousterout DG, Thakore PI, Moreb EA, Castellanos Rivera RM, Madhavan S, Pan X, Ran FA, Yan WX, et al. In vivo genome editing improves muscle function in a mouse model of Duchenne muscular dystrophy. Science. 2016; 351:403–407. [PubMed: 26721684]

Panesso MC, Shi M, Cho HJ, Paek J, Ye J, Moe OW, Hu MC. Klotho has dual protective effects on cisplatin-induced acute kidney injury. Kidney international. 2014; 85:855–870. [PubMed: 24304882]

Perez-Pinera P, Kocak DD, Vockley CM, Adler AF, Kabadi AM, Polstein LR, Thakore PI, Glass KA, Ousterout DG, Leong KW, et al. RNA-guided gene activation by CRISPR-Cas9-based transcription factors. Nature methods. 2013; 10:973–976. [PubMed: 23892895]

Pfister SX, Ashworth A. Marked for death: targeting epigenetic changes in cancer. Nature reviews Drug discovery. 2017; 16:241–263. [PubMed: 28280262]

Platt RJ, Chen S, Zhou Y, Yim MJ, Swiech L, Kempton HR, Dahlman JE, Parnas O, Eisenhaure TM, Jovanovic M, et al. CRISPR-Cas9 knockin mice for genome editing and cancer modeling. Cell. 2014; 159:440–455. [PubMed: 25263330]

Qi LS, Larson MH, Gilbert LA, Doudna JA, Weissman JS, Arkin AP, Lim WA. Repurposing CRISPR as an RNA-guided platform for sequence-specific control of gene expression. Cell. 2013; 152:1173–1183. [PubMed: 23452860]

Rafael JA, Tinsley JM, Potter AC, Deconinck AE, Davies KE. Skeletal muscle-specific expression of a utrophin transgene rescues utrophin-dystrophin deficient mice. Nature genetics. 1998; 19:79–82. [PubMed: 9590295]

Sanjana NE, Cong L, Zhou Y, Cunniff MM, Feng G, Zhang F. A transcription activator-like effector toolbox for genome engineering. Nature protocols. 2012; 7:171–192. [PubMed: 22222791]

Schaefer KA, Wu WH, Colgan DF, Tsang SH, Bassuk AG, Mahajan VB. Unexpected mutations after CRISPR-Cas9 editing in vivo. Nature methods. 2017; 14:547–548. [PubMed: 28557981]

Sicinski P, Geng Y, Ryder-Cook AS, Barnard EA, Darlison MG, Barnard PJ. The molecular basis of muscular dystrophy in the mdx mouse: a point mutation. Science. 1989; 244:1578–1580. [PubMed: 2662404]

Sienkiewicz D, Kulak W, Okurowska-Zawada B, Paszko-Patej G, Kawnik K. Duchenne muscular dystrophy: current cell therapies. Therapeutic advances in neurological disorders. 2015; 8:166–177. [PubMed: 26136844]

Suzuki K, Tsunekawa Y, Hernandez-Benitez R, Wu J, Zhu J, Kim EJ, Hatanaka F, Yamamoto M, Araoka T, Li Z, et al. In vivo genome editing via CRISPR/Cas9 mediated homology-independent targeted integration. Nature. 2016; 540:144–149. [PubMed: 27851729]

Swiech L, Heidenreich M, Banerjee A, Habib N, Li Y, Trombetta J, Sur M, Zhang F. In vivo interrogation of gene function in the mammalian brain using CRISPR-Cas9. Nature biotechnology. 2015; 33:102–106.

Tabebordbar M, Zhu K, Cheng JK, Chew WL, Widrick JJ, Yan WX, Maesner C, Wu EY, Xiao R, Ran FA, et al. In vivo gene editing in dystrophic mouse muscle and muscle stem cells. Science. 2016; 351:407–411. [PubMed: 26721686]

Takahashi Y, Wu J, Suzuki K, Martinez-Redondo P, Li M, Liao HK, Wu MZ, Hernandez-Benitez R, Hishida T, Shokhirev MN, et al. Integration of CpG-free DNA induces de novo methylation of CpG islands in pluripotent stem cells. Science. 2017; 356:503–508. [PubMed: 28473583]

Tanenbaum ME, Gilbert LA, Qi LS, Weissman JS, Vale RD. A protein-tagging system for signal amplification in gene expression and fluorescence imaging. Cell. 2014; 159:635–646. [PubMed: 25307933]

Tang DQ, Lu S, Sun YP, Rodrigues E, Chou W, Yang C, Cao LZ, Chang LJ, Yang LJ. Reprogramming liver-stem WB cells into functional insulin-producing cells by persistent expression of Pdx1- and

Author Manuscript Author Manuscript Author Manuscript Author Manuscript

Pdx1-VP16 mediated by lentiviral vectors. Laboratory investigation; a journal of technical methods and pathology. 2006; 86:83–93. [PubMed: 16294197]

Thakore PI, Black JB, Hilton IB, Gersbach CA. Editing the epigenome: technologies for programmable transcription and epigenetic modulation. Nature methods. 2016; 13:127–137. [PubMed: 26820547]

Tinsley JM, Potter AC, Phelps SR, Fisher R, Trickett JI, Davies KE. Amelioration of the dystrophic phenotype of mdx mice using a truncated utrophin transgene. Nature. 1996; 384:349–353. [PubMed: 8934518]

Vora S, Tuttle M, Cheng J, Church G. Next stop for the CRISPR revolution: RNA-guided epigenetic regulators. The FEBS journal. 2016; 283:3181–3193. [PubMed: 27248712]

Wehling-Henricks M, Li Z, Lindsey C, Wang Y, Welc SS, Ramos JN, Khanlou N, Kuro OM, Tidball JG. Klotho gene silencing promotes pathology in the mdx mouse model of Duchenne muscular dystrophy. Human molecular genetics. 2016; 25:2465–2482. [PubMed: 27154199]

Zincarelli C, Soltys S, Rengo G, Rabinowitz JE. Analysis of AAV serotypes 1–9 mediated gene expression and tropism in mice after systemic injection. Molecular therapy : the journal of the American Society of Gene Therapy. 2008; 16:1073–1080. [PubMed: 18414476]

Author Manuscript Author Manuscript Author Manuscript Author Manuscript

## Highlights

1. A CRISPR/Cas9 system transcriptionally activates endogenous target genes *in vivo*
2. Recruiting the transcriptional machinery causes *trans*-epigenetic remodeling
3. Inducing target gene expression causes physiological phenotypes in postnatal mammals
4. The system ameliorates symptoms associated with several mouse models of human diseases

Author Manuscript Author Manuscript Author Manuscript Author Manuscript

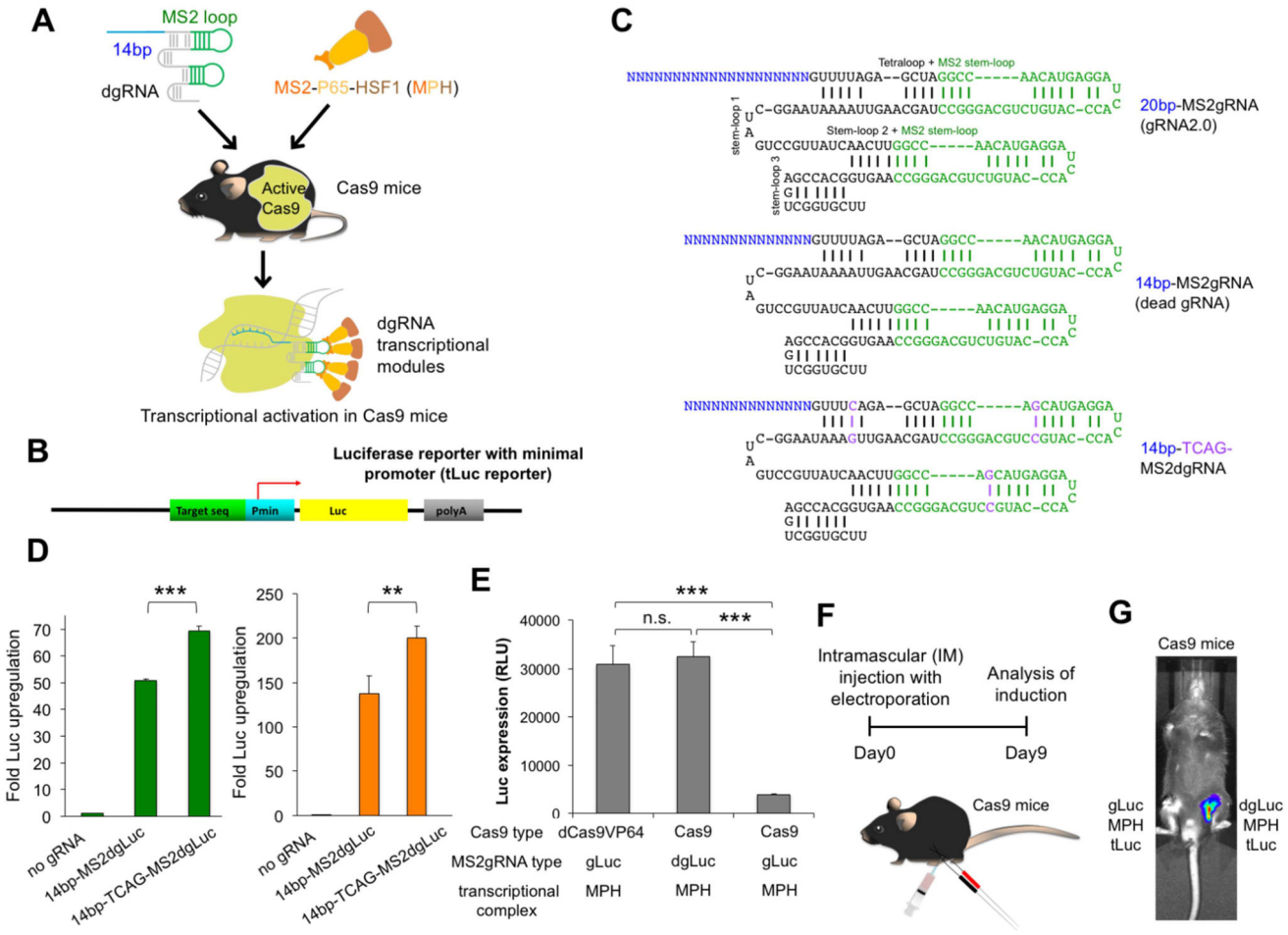


**Figure 1. A Modified dgRNA-Mediated CRISPR/Cas9 System for Target Gene Activation (CRISPR/Cas9 TGA System)**

**(A)** Schematic representation of how sgRNAs, which include a truncated 14-bp gRNA (dgRNA) and MS2 loops, are introduced with the MS2-P65-HSF1 (MPH) transcriptional activation complex, into Cas9-expressing mice for TGA. **(B)** The luciferase reporter (tLuc) includes dgRNA binding site (Target seq) followed by a minimal promoter (Pmin), a luciferase expression cassette (Luc), and a polyA termination signal. **(C)** Modified gRNAs. MS2gRNA (or gRNA 2.0) includes a wild type 20-bp gRNA and stem-loops for MPH binding. MS2dgRNA (or dead gRNA) includes a truncated 14-bp MS2gRNA that can recruit MPH to activate gene expression without inducing Cas9-mediated double-stranded breaks. Optimized MS2dgRNA (designated dgRNA) includes a 14-bp MS2dgRNA with modifications that enhance TGA. **(D)** dgRNA modification improves TGA of the tLuc reporter in 293 cells (left) and N2a cells that stably express Cas9 (right) ($n = 5$ each). **(E)** dgRNA modification results in Cas9/MPH-mediated TGA similar to that seen with the dCas9VP64/MPH/MS2gRNA SAM system in 293 cells ($n = 3$). TGA is weaker using wild-type gRNA, presumably because of DNA disruption. (**F**) Administration of the CRISPR/Cas9 TGA system *in vivo*. tLuc and dgLuc/MPH (or gLuc/MPH) plasmids were injected (IM) into Cas9 mice followed by electroporation. **(G)** *In vivo* imaging (day 9 post-IM

injection) revealed luciferase activity associated with the dgLuc/MPH construct, but not the gLuc/MPH control.

Author Manuscript Author Manuscript Author Manuscript Author Manuscript

Author Manuscript Author Manuscript Author Manuscript Author Manuscript

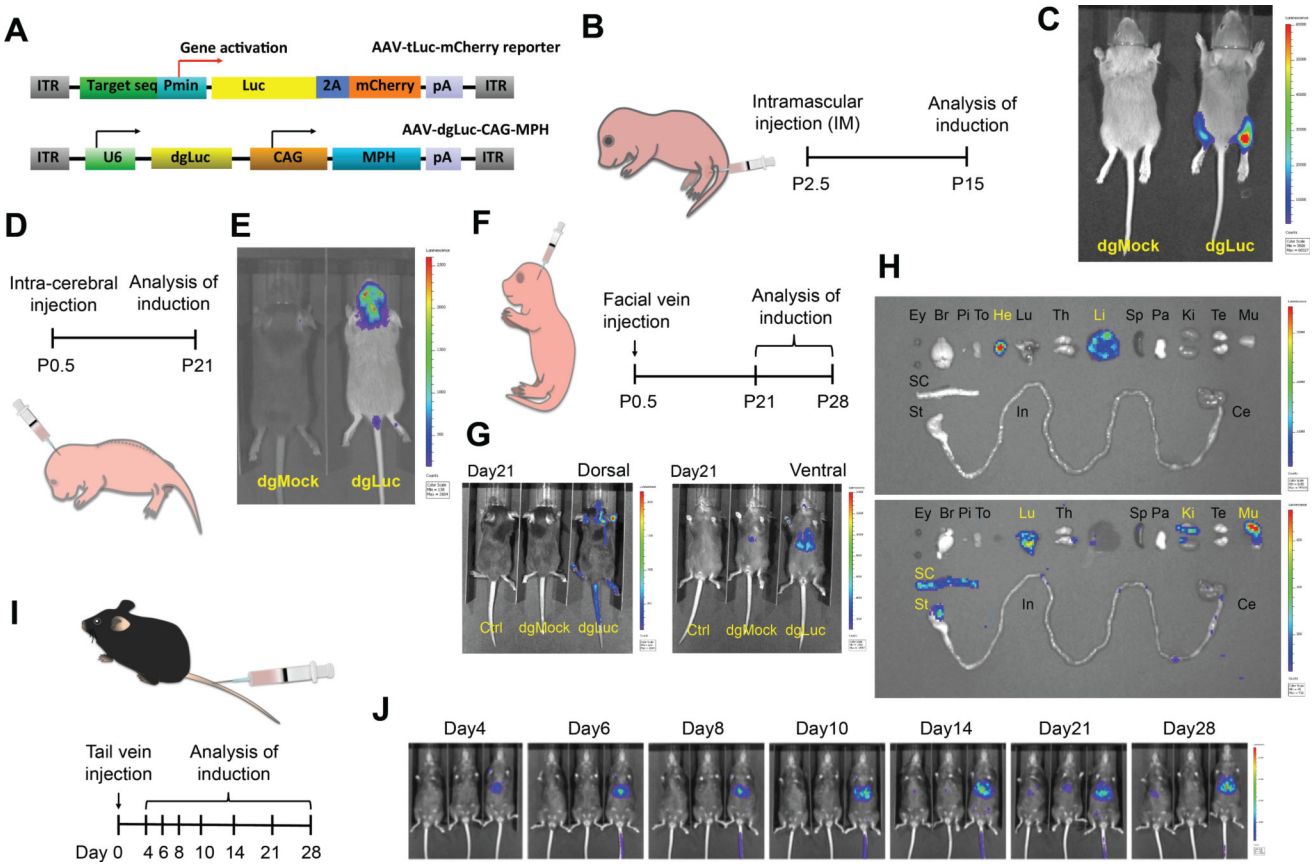


**Figure 2.** ***In Vivo*** **CRISPR/Cas9-Mediated Targeted Gene Activation of Reporters in Different Organs of Cas9 Mice**

**(A)** AAV-tLuc-mCherry and AAV-dgLuc-CAG-MPH vectors. **(B)** *In vivo* TGA of Luc reporter in Cas9 mice by IM injection at P2.5. **(C)** Luciferase imaging of Cas9 mice at P15 after IM injection of AAV-tLuc-mCherry and AAV-dgMock-MPH (dgMock) (left) or AAV-dgLuc-MPH (dgLuc) (right). **(D)** *In vivo* TGA of Luc reporter in Cas9 mice by intra-cerebral injection at P0.5. **(E)** Luciferase imaging of Cas9 mice at P21 after intra-cerebral injection of AAV-tLuc-mCherry and AAV-dgMock-MPH (left) or AAV-dgLuc-MPH (right). **(F)** *In vivo* TGA of reporter in neonatal Cas9 mice by facial vein injection at P0.5. **(G)** Luciferase imaging of Cas9 mice at P21 after facial vein injections of AAV-tLuc-mCherry and AAV9-dgMock-MPH (middle) or AAV-dgLuc-MPH (right). Non-injected mouse (Ctrl) is shown on the left. **(H)** *Ex vivo* luciferase imaging of eye (Ey), brain (Br), pituitary gland (Pi), tongue (To), heart (He), lung (Lu), thymus (Th), liver (Li), spleen (Sp), pancreas (Pa), kidney (Ki), testis (Te), muscle (Mu), spinal cord (SC), stomach (St), small intestine (In), and cecum (Ce) 28 days following facial vein injection. The luciferase signal is primarily in liver and heart (upper). Imaging the same tissues with a longer exposure time (lower) revealed lower levels of luciferase signal in Lu, Ki, Mu, and SC (Li and He were removed). **(I)** *In vivo* TGA of reporter in 11-week-old adult Cas9 mice through tail vein injection. **(J)** Luciferase imaging of Cas9 mice at 4, 6, 8, 10, 14, 21, and 28 days after tail vein injection of AAV-tLuc-mCherry and AAV-dgMock-MPH (middle) or AAV-dgLuc-MPH (right). Non-injected controls are shown (left).

Author Manuscript Author Manuscript Author Manuscript Author Manuscript

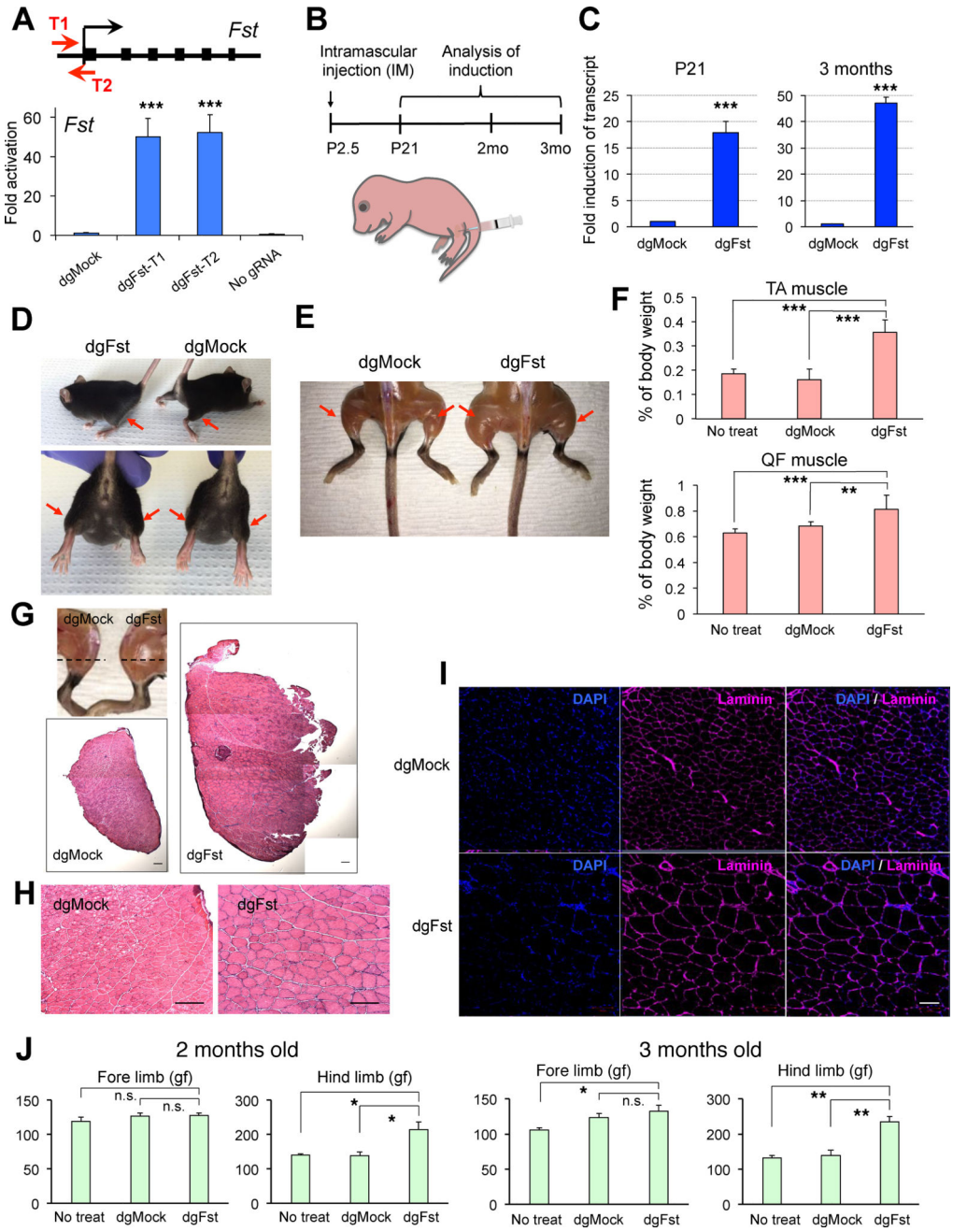


**Figure 3. Enhancement of Skeletal Muscle Mass by Cas9/dgRNA-MPH Mediated Follistatin Overexpression**

**(A)** The mouse *follistatin* (*Fst*) gene. dgRNA targets are indicated (red arrows). Cas9-expressing N2a cells were transfected with indicated dgRNAs and MPH. Levels of *Fst* expression were analyzed using qRT-PCR 3 days after transfections ($n = 3$). **(B)** *In vivo* TGA in neonatal Cas9 mice via IM injection of AAV-dgFst-T2-MPH (dgFst) or AAV-dgMock-MPH (dgMock) into hind limbs bilaterally at P2.5. **(C)** Cas9 mice received IM injections of AAV-dgFst-T2-MPH at P2.5, and qRT-PCR analysis of hindlimb muscle at P21 or 3 months for *Fst* induction. Gene expression fold-changes were quantified relative to

Author Manuscript Author Manuscript Author Manuscript Author Manuscript

AAV-dgMock-MPH controls ($n$ = 3). **(D and E)** Gross hindlimb muscle mass was increased in Cas9 mice injected with dgFst at P45 (D) or 3 months (E). **(F)** Muscle to body weight ratios for tibialis anterior (TA) and quadriceps femoris (QF) for no treatment controls ($n$ = 6) or 3 months after IM injection of dgMock ($n$ = 12) or dgFst ($n$ = 10). **(G)** Representative images of H&E stained TA muscles dissected 3 months after dgMock or dgFst injections. Scale bar, 200 μm. Image in upper-left corner indicates the position of TA dissection. **(H)** Higher magnification of sections in (G). Scale bar, 200 μm. **(I)** Immunostaining for Laminin in TA muscle section. Scale bar, 100 μm. **(J)** Grip strength test for fore and hind limbs of 2- or 3-month-old Cas9 mice (2-month-old: $n$ = 3, no treatment; $n$ = 5, dgMock; $n$ = 4, dgFst. 3-month-old: $n$ = 6, no treatment; $n$ = 5, dgMock; $n$ = 4, dgFst). See also Figure S2.

Author Manuscript Author Manuscript Author Manuscript Author Manuscript

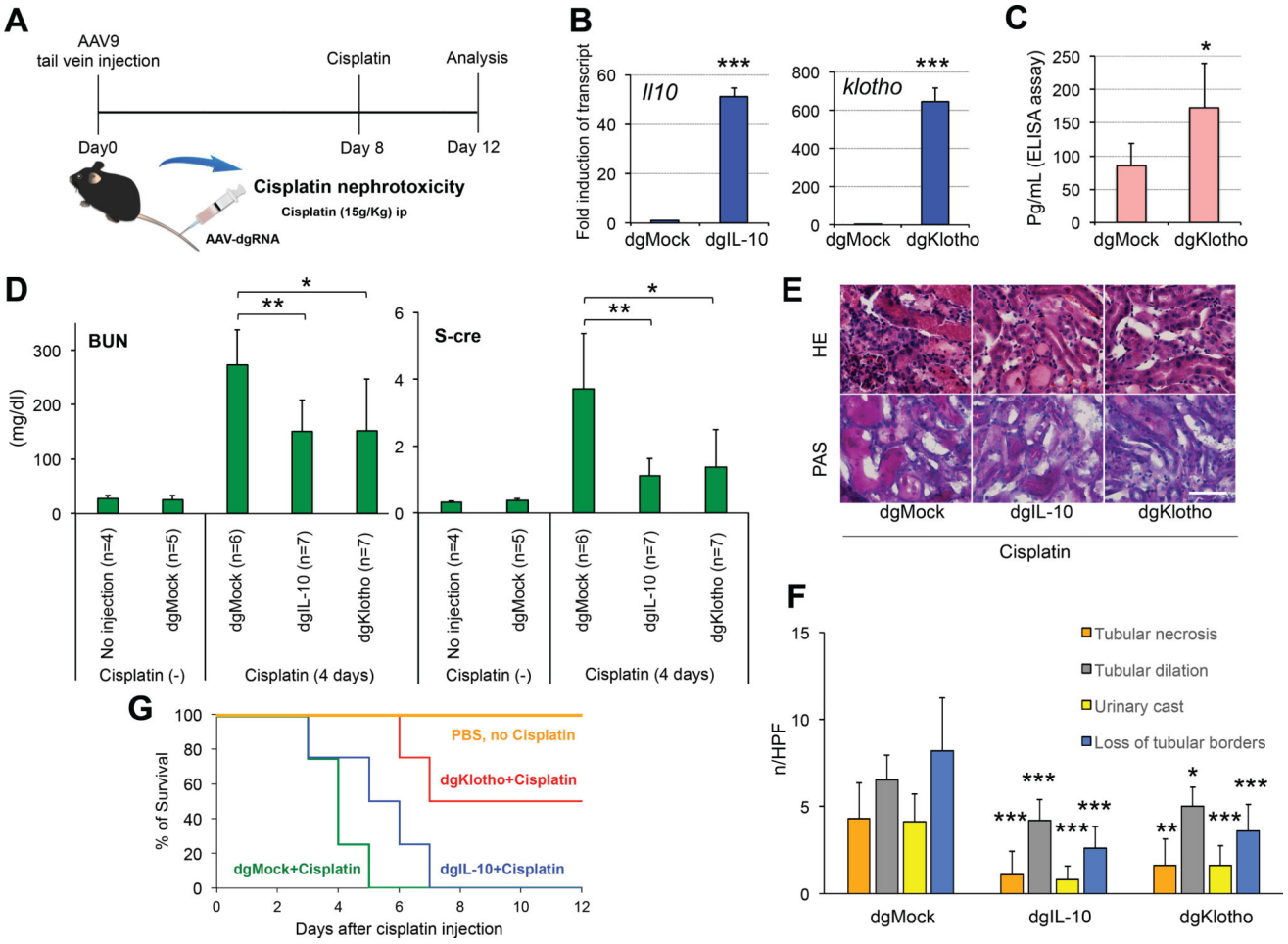


**Figure 4. Induction of IL-10 or Klotho Expression via CRISPR/Cas9 TGA System Ameliorates Acute Kidney Injury**

**(A)** Schematic of AAVs administration to Cas9 mice via tail-vein injection to prevent cisplatin-induced acute kidney injury (AKI). **(B)** qRT-PCR analyses of *Il10* and *klotho* expression in liver tissues from mice injected with AAV-dgIL-10-MPH ($n = 3$) or AAV-dgKlotho-MPH ($n = 3$). Fold enrichments were calculated relative to dgMock controls. **(C)** AAV-dgKlotho-MPH increased serum levels of Klotho protein relative to dgMock controls in cisplatin-treated mice ($n = 6$). Data are means ± SD. **(D)** Blood urea nitrogen (BUN) and serum creatinine (S-cre) levels in cisplatin-induced AKI mice were reduced by AAV-mediated IL-10 or Klotho overexpression. **(E and F)** Histological sections from indicated mice were subjected to H&E and PAS staining (E) and pathological features were quantified (F) (10~15 slides analyzed for 3–4 mice per group). Scale bar, 50 μm. **(G)** Survival curves of mice treated with the indicated AAV-dgRNAs for 8 days followed by a 17 g/Kg cisplatin challenge (via intraperitoneal injection; $n = 8$ for each group). See also Figure S3.

Author Manuscript Author Manuscript Author Manuscript Author Manuscript

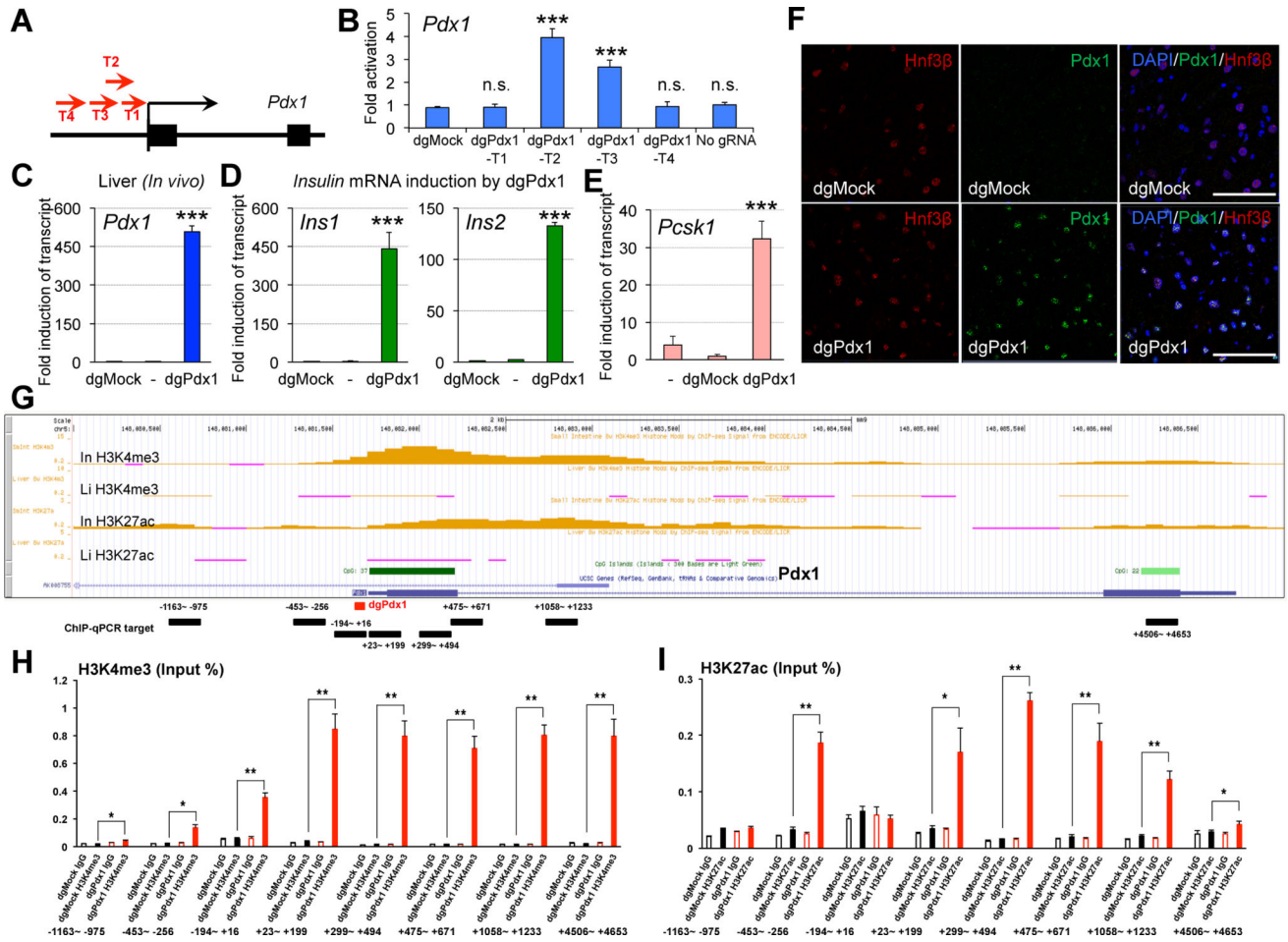


**Figure 5. *In Vivo* Epigenetic Activation of Pdx1 in Liver Cells Using the CRISPR/Cas9 TGA System Promotes Remodeling of Epigenetic Marks**

**(A)** The mouse *Pdx1* gene. gRNA targets are indicated (red arrows). **(B)** Cas9 mESCs were transfected with indicated gRNAs. Activation of *Pdx1* was analyzed by qRT-PCR 4 days after transfections. **(C)** qRT-PCR analysis of *in vivo Pdx1* gene induction in liver tissue of Cas9 mice that received a tail vein injection of AAV-dgPdx1-T2-MPH (13 days post-injection). Gene expression fold-change was quantified relative to AAV-dgMock-MPH controls. **(D and E)** qRT-PCR analysis of *in vivo* liver samples after *Pdx1* gene induction in (C). **(D)** Fold-change in *Ins1* and *Ins2* after *Pdx1* induction in liver. **(E)** Fold-change in *Pcsk1* after *Pdx1* induction in liver. **(F)** Immunofluorescence analyses of Pdx1 protein levels in liver tissue of mice injected with AAV-dgPdx1-T2-MPH or AAV-dgMock-MPH. Hepatocyte nuclear factor 3-beta (Hnf3β) (red) and Pdx1 (green) are shown. Scale bars, 50 μm. **(G–I)** dgRNA-mediated TGA system remodels epigenetic marks at *Pdx1* target loci *in vivo*. **(G)** Distribution of H3K4me3, H3K27ac, and CpG islands (green bars) at the *Pdx1* locus in small intestine (In) and liver (Li) tissue (UCSC genome browser). Black bars are ChIP-qPCR regions and red bar is the dgRNA target. **(H and I)** ChIP-qPCR analysis for H3K4me3 (H), H3K27ac (I), and IgG (negative control) in liver tissue of Cas9 mice that received tail vein injections of AAV-dgMock-MPH or AAV-dgPdx1-MPH. Relative real-time PCR values compared to input are shown. See also Figure S4.

Author Manuscript Author Manuscript Author Manuscript Author Manuscript

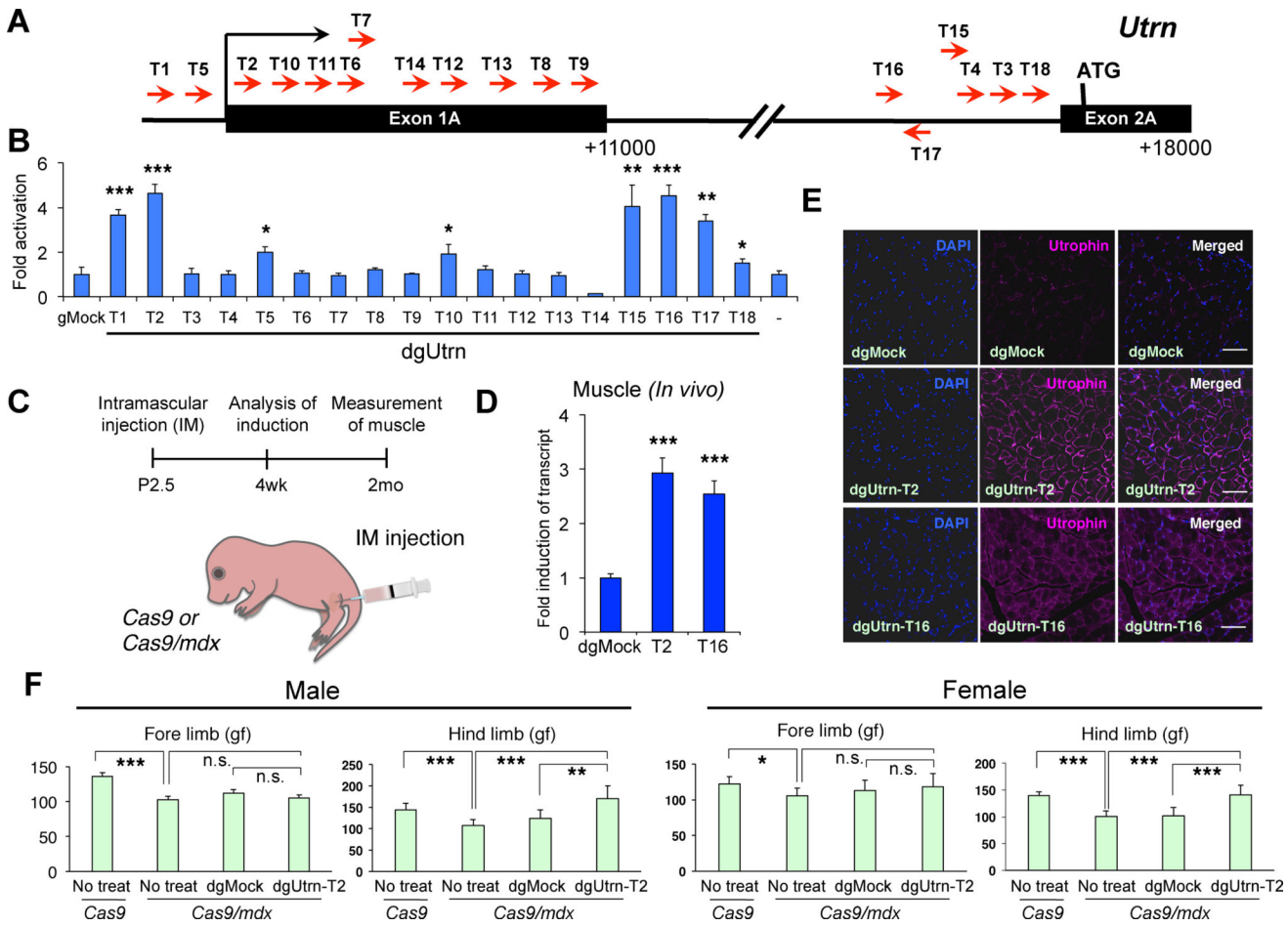


**Figure 6. CRISPR/Cas9 TGA of Utrophin Rescues Muscle Phenotypes of Dystrophin-Deficient Mice**

**(A)** Part of the mouse *utrophin* gene. dgRNA targets are indicated (red arrows). **(B)** Cas9 mESCs were transfected with indicated dgRNAs. Levels of *Utrn* activation were analyzed via qRT-PCR 3 days after transfections ($n = 3$). **(C)** *In vivo* TGA in neonatal Cas9 or Cas9/*mdx* mice via IM injection of AAV-dgUtrn-T2-MPH (dgUtrn-T2), AAV-dgUtrn-T16-MPH (dgUtrn-T16) or AAV-dgMock-MPH (dgMock) at P2.5. **(D)** qRT-PCR analysis of hind limb muscles of Cas9 mice 4 weeks after IM injections of AAV-dgUtrn at P2.5. Gene expression fold-changes were quantified relative to AAV-dgMock-MPH controls ($n = 3$). **(E)** Immunofluorescence of Utrophin in Cas9 mouse TA muscle injected with dgUtrn-T2, dgUtrn-T16, or dgMock (Utrophin, pink; DAPI, blue). Scale bars, 100 μm. **(F)** Physiological analyses of *mdx* mice in Cas9 transgenic background (Cas9/*mdx*) injected with AAV-dgUtrn-T2 or AAV-dgMock into hind limb muscle at P2.5. Grip strength test for fore limbs and hind limbs of 2-month-old mice ($n = 6$ (male) and 10 (female) for untreated Cas9 mice, $n = 9$ (male) and 6 (female) for untreated Cas9/*mdx* mice, $n = 8$ (male) and 9 (female) for AAV-dgMock injected Cas9/*mdx* mice, and $n = 7$ (male) and 10 (female) for AAV-dgUtrn-T2 injected Cas9/*mdx* mice.

Author Manuscript Author Manuscript Author Manuscript Author Manuscript

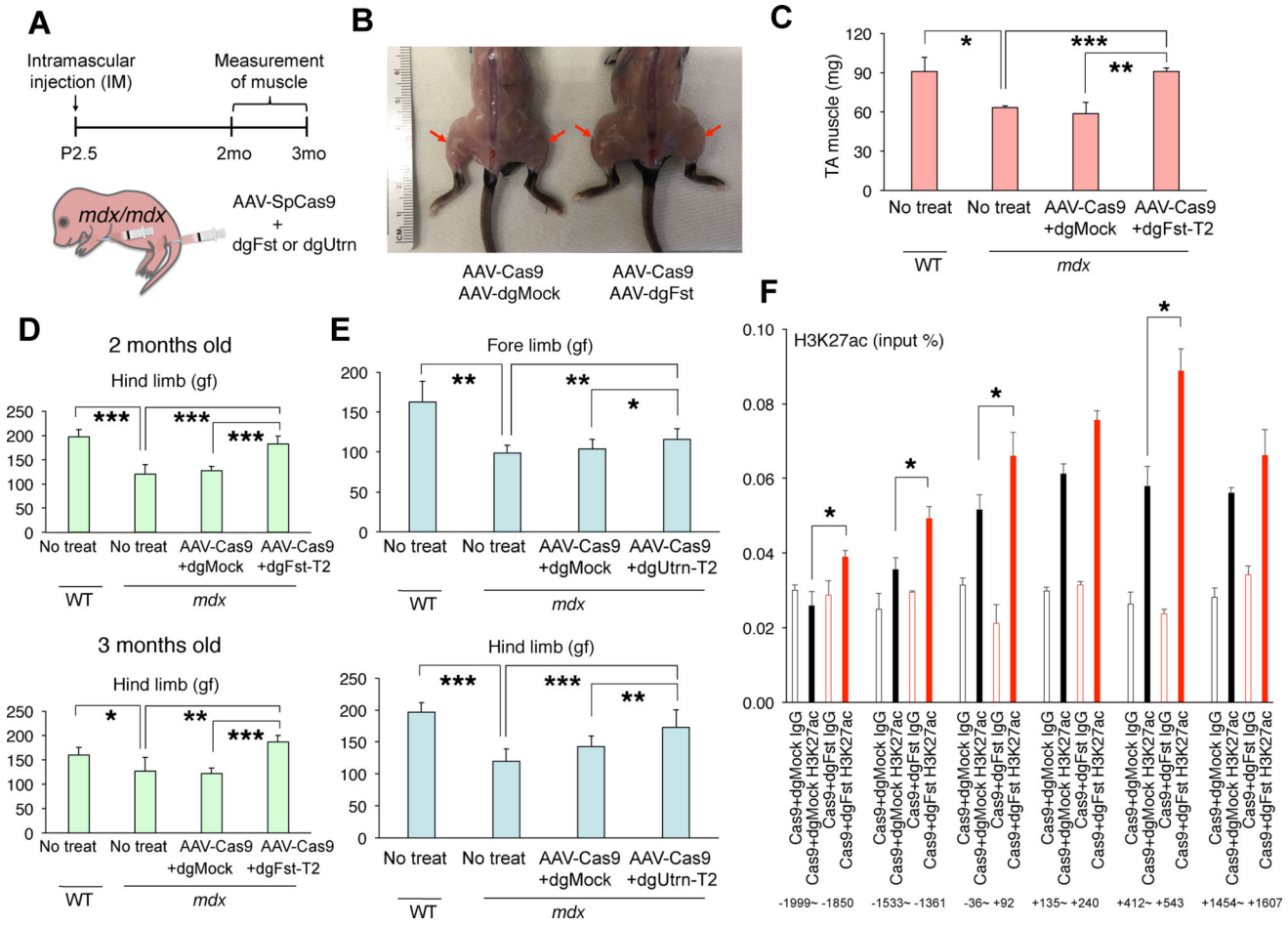


**Figure 7. Amelioration of Dystrophic Phenotypes of *Mdx* Mice Using a Dual AAV-CRISPR/Cas9 TGA System that Includes AAV-Cas9 and AAV-dgRNA-MPH**

**(A)** Neonatal IM co-injection of AAV-SpCas9 and AAV-dgFst-T2-MPH (dgFst-T2) or AAV-dgUtrn-T2-MPH (dgUtrn-T2) to treat *mdx* mice. **(B)** Three months post IM injection, gross hindlimb muscle mass was increased in *mdx* mice co-injected with AAV-SpCas9 and AAV-dgFst-T2 compared with AAV-dgMock controls. **(C)** TA muscle weight was increased in male *mdx* mice (3 months old) co-injected (IM) with AAV-SpCas9 and dgFst-T2 compared with no treatment and dgMock controls ($n = 4$ for each group). (**D**) Grip strength test for hind limbs of 2- and 3-month-old female mice (for 2-month-old mice: $n = 5$ for non-injected wild type, $n = 10$ for non-injected *mdx* mice, $n = 4$ for AAV-SpCas9+dgMock, $n = 6$ for AAV-SpCas9+dgFst-T2; for 3-month-old mice: $n = 11$ for non-injected wild type, $n = 7$ for non-injected *mdx* mice, $n = 3$ for AAV-SpCas9+dgMock, $n = 4$ for AAV-SpCas9+dgFst-T2). **(E)** Grip strength test for fore and hind limbs of 2-month-old female mice. AAVs were injected into both fore and hind limbs bilaterally ($n = 5$ for wild type mice, $n = 10$ for non-injected *mdx* mice, $n = 15$ for *mdx* mice co-injected with AAV-SpCas9 + AAV-dgMock, $n = 12$ for *mdx* mice co-injected with AAV-SpCas9 + AAV-dgUtrn-T2). **(F)** ChIP-qPCR analysis for H3K27ac and IgG (negative control) in muscle tissue of 3-month-old *mdx* mice that received IM co-injections of AAV-SpCas9 with either AAV-dgMock-MPH or AAV-dgFst-

T2-MPH. Relative real-time qPCR values compared to input are shown. The analytic regions for ChIP-qPCR are indicated at the bottom as shown in Figure S7D.

Author Manuscript Author Manuscript Author Manuscript Author Manuscript